Journal of Non-Newtonian Fluid Mechanics 251 (2018) 43–55

Contents lists available at ScienceDirect

Journal of Non-Newtonian Fluid Mechanics

journal homepage: www.elsevier.com/locate/jnnfm

Onsager-theory-based dynamic model for nematic phases of bent-core molecules and star molecules

Jie Xu*,[a], Pingwen Zhang[b]

[a] Department of Mathematics, Purdue University, West Lafayette 47907, USA
[b] LMAM & School of Mathematical Sciences, Peking University, Beijing 100871, China

ARTICLE INFO

Keywords:
Liquid crystals
Hydrodynamics
Kinetic theory
Tensor model
Quasi-equilibrium closure approximation
Bent-core molecules
Star molecules

ABSTRACT

We construct the molecular model and the tensor model for the dynamics of the nematic phases of bent-core molecules and star molecules in incompressible fluid. We start from the molecular interaction and the molecule–fluid friction, and write down a general formulation based on the molecular shape and the free energy. Then we incorporate an Onsager-theory-based static tensor model to obtain the dynamic molecular model fully determined by the molecular architecture. The tensor model is obtained by adopting the quasi-equilibrium approximation that maintains energy dissipation. For bent-core molecules and star molecules that have the same molecular symmetry, the form of the model is identical. The molecular architecture is differentiated by the coefficients that are derived as functions of molecular parameters. Numerical simulation is carried out for the shear flow problem using both the molecular and the tensor models, focusing on the effect of altering molecular architecture. When the equilibrium phase is biaxial, novel flow modes are found, and the flow mode sequences show delicate dependence on the molecular architecture. The tensor model proves to exhibit all the flow modes found in the molecular model.

1. Introduction

The liquid crystalline flows are studied extensively in the last few decades. The majority of works focus on rod-like molecules that can exhibit uniaxial nematic phase in equilibrium. The earliest and simplest approach is the macroscopic Ericksen–Leslie theory [23], in which the orientation is described by a unit vector. However, this approach is insufficient to investigate singular phenomena, such as defects. For the microscopic approach, Doi [10] established the kinetic equation of the density function (the Smoluchowski equation), which we call the molecular model. Doi theory has been applied to study the spatially homogeneous shear flow problem for rod-like molecules [12,13,21,22]. It has also been extended to inhomogeneous flows [14,27,40,46,47]. Despite its great success, the simulation is time-consuming, making its application to inhomogeneous flows rather restricted. To reduce the dimension of variables, many works aim to construct models in which the orientation is described by tensors. Apart from some phenomenological tensor models [4,29], most tensor models are obtained by closure approximation of Doi theory [2,3,8,11,16,18–20,39,45]. With various closure approximations for different types of flows, the tensor models have proved to be able to capture the phenomena in the molecular model, although no one closure approximation can recover all the phenomena.

When the molecule is not axisymmetric, the phase behavior can become very complicated. As a representative, bent-core molecules have attracted much attention. Even when restrained to nematics phases, they have proved to show the biaxial nematic phase [1,26] and the modulated twist-bend phase [6,9,28]. The nematic phase behavior of bent-core molecules has also been discussed theoretically [5,15,31,32,37]. The most eminent difference between bent-core molecules and rod-like molecules is that numerous experiments have shown that the phase behavior is sensitively dependent on specific molecular architecture [36], which is far from well-understood. The dynamics of bent-core molecules is thus expected to be fascinating. In particular, it is extremely desirable to understand the connection between the molecular architecture and the macroscopic flow pattern.

In [17], a three-level schema is proposed for the modeling of rod-like liquid crystals, applicable for both static and dynamic theory. Starting from the molecular model, one can derive the tensor model, then the vector model (Oseen–Frank and Ericksen–Leslie theory), with all the coefficients determined by molecular parameters and the energy dissipation retained. We have applied the approach to the static theory of rigid molecules with achiral twofold symmetry, two of which are bent-core molecules and star molecules (see Fig. 1). For molecular

* Corresponding author.
E-mail addresses: xu924@purdue.edu (J. Xu), pzhang@pku.edu.cn (P. Zhang).

https://doi.org/10.1016/j.jnnfm.2017.11.005
Received 7 May 2017; Received in revised form 18 October 2017; Accepted 17 November 2017
Available online 21 November 2017
0377-0257/

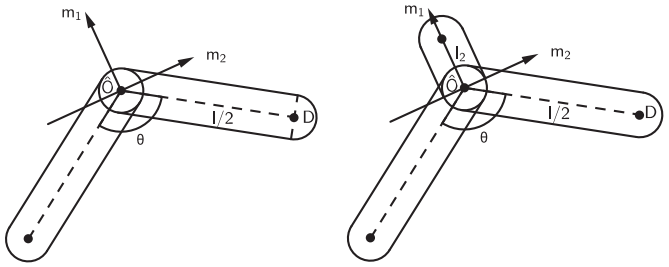

Fig. 1. Bent-core molecule and star molecule.

interaction, we consider the Onsager theory, i.e. adopt the hardcore interaction that is determined by the molecular architecture. We have studied the order parameters and homogeneous phases [43], where we have shown that three tensors, one first-order (vector) and two second-order symmetric, shall be chosen. The elastic energy is derived in [42] to investigate modulated nematic phases. It also enables us to examine how the elastic constants are affected by molecular architecture [44]. The key point is that the order parameters and the form of the free energy are determined by molecular symmetry. In other words, for bent-core and star molecules, or other molecules with the same symmetry such as T-shaped, W-shaped, equilateral-triangular-shaped, and circular-arc-shaped, the order parameters and the form of free energy are identical. The molecular architecture, which is a crucial factor as the experiments indicate, is distinguished by the coefficients that are derived as functions of molecular parameters.

Now we turn to the dynamics of non-axisymmetric liquid crystals. Macroscopic dynamic models have been proposed for the biaxial nematic phase [7,24,30] as an extension of the Ericksen–Leslie theory. Their applications are even more limited than the Ericksen–Leslie theory, because multiple nematic phases may coexist. Meanwhile, to our knowledge, no tensor model has been proposed. As for the microscopic approaches, the Smoluchowski equation is adopted to investigate the dynamics of ellipsoids [34,35] and bent-core molecules [33]. These works present some inspiring results on the homogeneous shear flow problem, obtaining several flow modes different from rod-like molecules. Despite this, they are far from sufficient for the aim to build connection between molecular architecture and flow pattern. One apparent limitation is that the model in these works includes only the local biaxial interaction. A less noticeable but much more serious drawback is the inconsistency of the coefficients with the molecular architecture. Some coefficients are phenomenological, and some are derived from different molecular architecture. It makes the model unable to definitely claim that certain flow patterns are resulted from a certain molecule, because it is solely the coefficients that differentiate molecular architecture. The results also show inconsistency in symmetry. The appearance of nonzero mixed second moments does not comply the twofold molecular symmetry, which we will discuss in our numerical results. These shortcomings shall be overcome in this paper.

The main goal of this paper is to establish a dynamic model that clearly reflects the effect of molecular architecture on flow patterns. We consider the hardcore molecular interaction and the friction between molecules and the fluid. For the molecule–fluid friction, we write down the general formulation. Then we carefully adopt the same molecular architecture as in the static model, so that we can build the free energy into the dynamic model consistently. In this way, we are able to write down the molecular model, with the energy dissipation law, fully based on molecular architecture and physical parameters. Since it makes no difference in derivation, we write down a generic model that is available for future applications to inhomogeneous flows. Similar to the static model, for bent-core molecules and star molecules, the dynamic model shares the same form because they have the same molecular symmetry. This is also the case if we consider other types of microscopic interactions. The molecular architecture is differentiated by the coefficients that are deduced from molecular parameters.

We then derive the dynamic tensor model that describes the orientation more concisely, which has not been considered in literature and is our second goal. We deduce the equation of the three tensors appearing in the free energy from the Smoluchowski equation. The high-order tensors appearing in the tensor model are expressed by the three tensors using quasi-equilibrium approximation, a generalization of the Bingham closure, which keeps the energy dissipation law. Also, the tensor model inherits the property that the form and coefficients are determined by the molecular symmetry and the molecular parameters, respectively.

For the numerical simulation, we restrain our attention to the shear flow problem. We examine the flow modes for both bent-core molecules and star molecules, illustrating the ability of the model to systematically study the variation of flow modes resulting from adjusting molecular architecture. The results we obtain are consistent with the molecular symmetry. In particular, we choose the parameters in the vicinity of the uniaxial–biaxial phase boundary in quiescent fluid, which is not studied previously. We find that the flow mode sequences do not vary much in uniaxial regions, but exhibit big change in the biaxial region. Moreover, in the biaxial region, we find flow modes that do not resemble any one reported previously. Also, we compare the results obtained from the molecular model and the tensor model. The tensor model is able to exhibit all the flow modes found in the molecular model, although under different parameters. The sequence is mostly identical at low shear rates.

The paper is organized as follows. In Section 2 we derive the molecular model. In Section 3 we derive the tensor model and prove the energy dissipation along with the quasi-equilibrium closure approximation. In Section 4 we use both the molecular model and the tensor model to examine the shear flow problem. Concluding remarks are given in Section 5.

2. Molecular model

2.1. Notations

We view the molecules that form liquid crystalline states as fully rigid. Thus, we may choose a body-fixed orthogonal frame $(\hat{O}; \boldsymbol{m}_1, \boldsymbol{m}_2, \boldsymbol{m}_3)$ to describe the position and the orientation of a molecule. In a space-fixed orthogonal coordinate system $(O; \boldsymbol{e}_1, \boldsymbol{e}_2, \boldsymbol{e}_3)$, they can be expressed in terms of $\boldsymbol{x} = \overrightarrow{O\hat{O}}$ and a three-dimensional proper rotation $P \in SO(3)$. In the language of matrix, P is a 3×3 orthogonal with $\det P = 1$ such that

$$(\boldsymbol{m}_1, \boldsymbol{m}_2, \boldsymbol{m}_3) = (\boldsymbol{e}_1, \boldsymbol{e}_2, \boldsymbol{e}_3)P. \tag{2.1}$$

The elements of $P^T = (m_{ij})$ are the components of $\boldsymbol{m}_i$, denoted by $m_{ij} = \boldsymbol{m}_i \cdot \boldsymbol{e}_j$.

In some cases, we need to specify a point on the molecule, and we use its coordinates $\hat{\boldsymbol{r}}$ in the body-fixed frame $(\hat{O}; \boldsymbol{m}_1, \boldsymbol{m}_2, \boldsymbol{m}_3)$. Every $P \in SO(3)$ can be expressed by Euler angles α, β, γ:

$$P(\alpha, \beta, \gamma) = \begin{pmatrix} \cos\alpha & -\sin\alpha\cos\gamma & \sin\alpha\sin\gamma \\ \sin\alpha\cos\beta & \cos\alpha\cos\beta\cos\gamma & -\cos\alpha\cos\beta\sin\gamma \\ & -\sin\beta\sin\gamma & -\sin\beta\cos\gamma \\ \sin\alpha\sin\beta & \cos\alpha\sin\beta\cos\gamma & -\cos\alpha\sin\beta\sin\gamma \\ & +\cos\beta\sin\gamma & +\cos\beta\cos\gamma \end{pmatrix}, \tag{2.2}$$

with

$$\alpha \in [0, \pi], \quad \beta, \gamma \in [0, 2\pi).$$

The uniform probability measure on SO_3 is given by

$$\mathrm{d}\nu = \frac{1}{8\pi^2}\sin\alpha \mathrm{d}\alpha\mathrm{d}\beta\mathrm{d}\gamma.$$

For the notations of tensors, we use the summation over repeated indices. The product of several tensors without operators is recognized as tensor product: $\boldsymbol{m}_1\boldsymbol{m}_2\boldsymbol{m}_3$ represents a third order tensor with the (i, j, k) component $m_{1i}m_{2j}m_{3k}$. If a tensor contraction involves first or second order tensor, we also use the single and double dots: suppose we have a first order tensor $\boldsymbol{p}$, a second order tensor Q, and a fourth order tensor R, then

$$(Q\cdot\boldsymbol{p})_i = Q_{ij}p_j, \quad (\boldsymbol{p}\cdot R)_{jkl} = p_i R_{ijkl}, \quad (Q\colon R)_{kl} = Q_{ij}R_{ijkl}. \tag{2.3}$$

To describe the number of molecules with certain position $\boldsymbol{x}$ and orientation P, we introduce the density function $f(\boldsymbol{x}, P)$. Moreover, we split $f(\boldsymbol{x}, P)$ into the local concentration $c(\boldsymbol{x})$ and the orientational distribution $\rho(\boldsymbol{x}, P)$,

$$c(\boldsymbol{x}) = \int \mathrm{d}\nu f\left(\boldsymbol{x}, P\right), \qquad \rho\left(\boldsymbol{x}, P\right) = f\left(\boldsymbol{x}, P\right)/c(\boldsymbol{x}). \tag{2.4}$$

The notation $<\cdot>$ represents the average about $\rho(\boldsymbol{x}, P)$,

$$\langle(\cdot)\rangle = \int \mathrm{d}\nu(\cdot)\rho(\boldsymbol{x}, P).$$

The differential operators on $SO(3)$ are involved when discussing the motion of the rigid molecules. In specific, we use L_i to denote the derivatives along the infinitesimal rotation about $\boldsymbol{m}_i$. The operators L_i can be expressed by derivatives of Euler angles,

$$L_1 = \frac{\partial}{\partial\gamma}, \tag{2.5}$$

$$L_2 = \frac{-\cos\gamma}{\sin\alpha}\left(\frac{\partial}{\partial\beta} - \cos\alpha\frac{\partial}{\partial\gamma}\right) + \sin\gamma\frac{\partial}{\partial\alpha}, \tag{2.6}$$

$$L_3 = \frac{\sin\gamma}{\sin\alpha}\left(\frac{\partial}{\partial\beta} - \cos\alpha\frac{\partial}{\partial\gamma}\right) + \cos\gamma\frac{\partial}{\partial\alpha}. \tag{2.7}$$

Denote $L = (L_1, L_2, L_3)^T$. If a vector-valued function $\boldsymbol{a}(P)$ is expressed as $\boldsymbol{a}(P) = a_1(P)\boldsymbol{m}_1 + a_2(P)\boldsymbol{m}_2 + a_3(P)\boldsymbol{m}_3$, then the divergence is defined by

$$L\cdot\boldsymbol{a} = L_1a_1 + L_2a_2 + L_3a_3.$$

We may verify the following properties using the above definition. Acting the operators on m_{ij}, we have

$$L_i\boldsymbol{m}_j = \epsilon_{ijk}\boldsymbol{m}_k. \tag{2.8}$$

Here we use the Levi–Civita symbol,

$$\epsilon_{k_1k_2k_3} = \begin{cases} 1, & (k_1k_2k_3) = (123), (231), (312); \\ -1, & (k_1k_2k_3) = (132), (213), (321); \\ 0, & \text{otherwise.} \end{cases}$$

The operators also satisfy the integration by parts on $SO(3)$,

$$\int \mathrm{d}\nu f\left(L_i g\right) = -\int \mathrm{d}\nu\left(L_i f\right)g. \tag{2.9}$$

2.2. General formulation

The motion of rigid molecules includes translation and rotation, driven by molecular interaction and molecule–fluid interaction. In general, the translation and rotation can be coupled. But in what follows, we will deduce them separately under various approximations. To let our discussion be specific, we assume that a rigid molecule consists of spheres of the diameter D and the mass m_0. In this case, the architecture of a molecule is given by the number density of the sphere centers $\hat{\rho}(\hat{\boldsymbol{r}})$ in the body fixed frame $(\widehat{O}; \boldsymbol{m}_1, \boldsymbol{m}_2, \boldsymbol{m}_3)$, and we assume that the center of mass is located at $\widehat{O}$. The rigid molecules are dissolved in incompressible viscous fluid, and the molecule-fluid interaction stems from the friction between them. The frictional force between a sphere and the fluid is proportional to the relative velocity, given by $\boldsymbol{F} = -\zeta\boldsymbol{V}$, where $\zeta = 3\pi D\eta_0$ is the friction constant.

The molecular interaction induces a potential field $\mu(\boldsymbol{x}, P)$ given by the functional derivative

$$\mu = \frac{\delta F[f]}{\delta f}, \tag{2.10}$$

where $F[f]$ represents the free energy of a system with the number density $f(\boldsymbol{x}, P)$ of rigid molecules. The free energy includes the contribution of the entropy and pairwise interaction,

$$F[f] = F_{entropy}[f] + F_r[f], \tag{2.11}$$

where

$$F_{entropy} = k_BT\int \mathrm{d}\boldsymbol{x}\mathrm{d}\nu\ f\log f. \tag{2.12}$$

For bent-core molecules and star molecules, we will give the expression of F_r later.

2.2.1. Smochulowski equation

In general, the Smochulowski equation for the rigid molecules can be written as

$$\frac{\partial f}{\partial t} = -\nabla\cdot(f\boldsymbol{w}) - L\cdot(f\boldsymbol{\omega}). \tag{2.13}$$

Here, for the molecule at the position $\boldsymbol{x}$ and the orientation P, we use $\boldsymbol{w}(\boldsymbol{x}, P)$ to denote the velocity of the center of mass, and $\boldsymbol{\omega}(\boldsymbol{x}, P)$ to denote the angular velocity. For both of them, we split the contribution of molecular interaction, $\boldsymbol{w}_m$, $\boldsymbol{\omega}_m$, and fluid–molecule interaction, $\boldsymbol{w}_f$, $\boldsymbol{g}$, by writing

$$\boldsymbol{w} = \boldsymbol{w}_m + \boldsymbol{w}_f, \quad \boldsymbol{\omega} = \boldsymbol{\omega}_m + \boldsymbol{g}.$$

We start from the rotation resulted from the molecular interaction. To derive this term, we assume that a molecule is rotating in the quiescent fluid, with the angular velocity $\boldsymbol{\omega}_m$ round the center of mass. The torque generated by the friction between a molecule and the quiescent fluid is the sum of frictional torque on each sphere,

$$-\boldsymbol{N} = \zeta\int \mathrm{d}\hat{\boldsymbol{r}}\hat{\rho}(\hat{\boldsymbol{r}})\hat{\boldsymbol{r}}\times(\boldsymbol{\omega}_m\times\hat{\boldsymbol{r}}) = \frac{\zeta}{m_0}\boldsymbol{I}\boldsymbol{\omega}_m, \tag{2.14}$$

where $\boldsymbol{I}$ is the moment of inertia of a molecule, calculated as

$$\boldsymbol{I} = m_0\int \mathrm{d}\hat{\boldsymbol{r}}\hat{\rho}(\hat{\boldsymbol{r}})(|\hat{\boldsymbol{r}}|^2 - \hat{\boldsymbol{r}}\hat{\boldsymbol{r}}). \tag{2.15}$$

On the other hand, suppose the molecule is doing an infinitesimal rotation $\delta P = \delta t\boldsymbol{\phi}\times P$. Then the work done by the frictional torque is $-\boldsymbol{N}\cdot\boldsymbol{\phi}\delta t$, and shall equal to the variation of potential. Therefore,

$$\boldsymbol{N}\cdot\boldsymbol{\phi}\delta t = \mu(P+\delta P) - \mu(f) = \delta t\boldsymbol{\phi}\cdot L\mu,$$

yielding $\boldsymbol{N} = L\mu$. Comparing it with (2.14), we have

$$\boldsymbol{\omega}_m = -\frac{m_0}{\zeta}\boldsymbol{I}^{-1}L\mu.$$

If we carefully choose $\boldsymbol{m}_i$ such that $\boldsymbol{I}$ is diagonal in the body-fixed frame, then we can write

$$\boldsymbol{\omega}_m = \sum_{i=1}^{3}\omega_i\boldsymbol{m}_i = -\sum_{i=1}^{3}(D_iL_i\mu)\boldsymbol{m}_i,$$

where the diffusion coefficients are given by

$$D_i = \frac{m_0}{\zeta I_{ii}}. \tag{2.16}$$

Note that $\boldsymbol{\omega}_m$ actually gives a diffusion term $L\cdot(m_0\zeta^{-1}\boldsymbol{I}^{-1}fL\mu)$ in the Smoluchowski equation. Define

$$V = \frac{\delta F_r}{\delta f}, \tag{2.17}$$

then we can split μ as

$$\mu = k_B T(\log f + 1) + V. \tag{2.18}$$

and the diffusion term can also be written as

$$\sum_{i=1}^{3} D_i[k_B T L_i^2 f + L_i(f L_i V)]. \tag{2.19}$$

Similarly, we derive $\boldsymbol{w}_m$ by considering the translation of a molecule in the quiescent fluid. Generally, $\boldsymbol{w}_m$ can be written as

$$\boldsymbol{w}_m = -\boldsymbol{J}(k_B T \nabla f + f \nabla V), \tag{2.20}$$

where the diffusion coefficient $\boldsymbol{J}$ is a 3×3 positive matrix. To derive $\boldsymbol{J}$, we need to consider the hydrodynamic interaction, namely the interaction of different spheres through the fluid, which can be done using the Kirkwood theory (see [10]). In Appendix, we will outline how to use the Kirkwood theory to calculate $\boldsymbol{J}$ and present the result for bent-core molecules. As a simple approximation, if we ignore the hydrodynamic interaction, then $\boldsymbol{J}$ will be a multiple of the identity matrix.

Next we derive the translation and rotation generated by molecule–fluid interaction. Now we need to consider the motion of a molecule driven by the fluid with inhomogeneous velocity. We require that the velocity of the center of mass, $\boldsymbol{w}_f$, and the angular velocity, $\boldsymbol{g}$, minimize the frictional work. Denote by $\boldsymbol{u}(\hat{\boldsymbol{r}})$ and $\boldsymbol{u}_p(\hat{\boldsymbol{r}})$ the velocity of the fluid and the sphere at the point $\hat{\boldsymbol{r}}$, respectively. Then the frictional work of the fluid and the molecule can be written as

$$W = \zeta \int \mathrm{d}\hat{\boldsymbol{r}} \hat{\rho}(\hat{\boldsymbol{r}}) |\boldsymbol{u} - \boldsymbol{u}_p|^2. \tag{2.21}$$

Note that $\boldsymbol{u}_p = \boldsymbol{w}_f - \boldsymbol{g} \times \hat{\boldsymbol{r}}$. Since the scale of rigid molecule is much smaller than the fluid field, we may suppose that the flow is linear. In other words, if we denote $\kappa_{ij} = \partial_j u_i$, then we may assume

$$\boldsymbol{u}(\hat{\boldsymbol{r}}) = \kappa \cdot \hat{\boldsymbol{r}} + \boldsymbol{u}_0.$$

Here, $\boldsymbol{u}_0$ is the velocity at $\boldsymbol{x}$, where $\widehat{O}$ is located. By minimizing (2.21), we deduce that

$$\boldsymbol{w}_f = \boldsymbol{u}_0, \quad \boldsymbol{g} = m_0 \boldsymbol{I}^{-1} \int \mathrm{d}\hat{\boldsymbol{r}} \hat{\rho}(\hat{\boldsymbol{r}})(\hat{\boldsymbol{r}} \times \kappa \cdot \hat{\boldsymbol{r}}). \tag{2.22}$$

If we denote the fluid velocity by $\boldsymbol{v}(\boldsymbol{x})$, then we may write

$$\boldsymbol{w}_f = \boldsymbol{u}_0 = \boldsymbol{v}. \tag{2.23}$$

Summarizing the derivation above, the Smoluchowski equation can be rewritten as follows,

$$\frac{\partial f}{\partial t} + \nabla \cdot (f\boldsymbol{v}) = \nabla \cdot (\boldsymbol{J}(k_B T \nabla f + f \nabla V)) + L \cdot [(D_0 \boldsymbol{I}^{-1})(k_B T L f + f L V)] - L \cdot (\boldsymbol{g} f). \tag{2.24}$$

2.2.2. Momentum equation

The incompressibility gives

$$\nabla \cdot \boldsymbol{v} = 0. \tag{2.25}$$

The momentum equation is written as

$$\rho_s \left(\frac{\partial \boldsymbol{v}}{\partial t} + \boldsymbol{v} \cdot \nabla \boldsymbol{v} \right) = -\nabla p + \nabla \cdot \tau + \boldsymbol{F}_e, \tag{2.26}$$

where ρ_s is the density of the fluid, $\boldsymbol{F}_e$ is the external force, and $\tau = \tau_e + \tau_v$ is the stress, divided into the elastic and the viscous part. The elastic stress τ_e and the external force $\boldsymbol{F}_e$ can be derived from the principle of virtual work. Because the derivation is standard and can be found in literature [10], we only list the results here. The external force $\boldsymbol{F}_e$ is given by

$$\boldsymbol{F}_e = -\int \mathrm{d}\nu \ \nabla \mu(f) f = -c \langle \nabla \mu \rangle, \tag{2.27}$$

where we recall that c is the concentration. For τ_e, if we express $\boldsymbol{g}$ as

$$\boldsymbol{g} = \kappa_{jk} : (\alpha_i)_{jk} \boldsymbol{m}_i, \tag{2.28}$$

then

$$(\tau_e)_{jk} = c \langle (\alpha_i)_{jk} L_i \mu \rangle. \tag{2.29}$$

When $\boldsymbol{I}$ is diagonal, by (2.22), we deduce

$$\alpha_i = m_0 I_{ii}^{-1} \int \mathrm{d}\hat{\boldsymbol{r}} \hat{\rho}(\hat{\boldsymbol{r}}) \hat{\boldsymbol{r}} (\boldsymbol{m}_i \times \hat{\boldsymbol{r}}). \tag{2.30}$$

The viscous stress can be expressed as

$$\tau_v = 2\eta(\kappa + \kappa^T) + \tau_{vf}. \tag{2.31}$$

The first term is the contribution of the friction in the fluid itself, and τ_{vf} is the contribution of the friction between the fluid and the molecules, determined by the following equation

$$c \langle W \rangle = \kappa : \tau_{vf}, \tag{2.32}$$

where W is given by (2.21) with $\boldsymbol{g}$ taking (2.22).

The whole system is described by (2.24)–(2.26), with the terms given by (2.16), (2.22), (2.27), (2.29), (2.32). It is worth noting that all the terms are derived from the distribution of sphere centers $\hat{\rho}(\hat{\boldsymbol{r}})$ and the free energy $F[f]$.

2.2.3. Energy dissipation law

The energy of the system includes the free energy (2.11) and the kinetic energy of the fluid,

$$\int \mathrm{d}\boldsymbol{x} \frac{\rho_s}{2} |\boldsymbol{v}|^2 + F[f].$$

Now let us prove the energy dissipation law. For simplicity, we omit $k_B T$ in the following. We have

$$\begin{aligned}
&\frac{\mathrm{d}}{\mathrm{d}t}\left(\int \mathrm{d}\boldsymbol{x} \frac{\rho_s}{2} |\boldsymbol{v}|^2 + F[f] \right) \\
&= \int \mathrm{d}\boldsymbol{x} \left(\rho_s \boldsymbol{v} \cdot \frac{\partial \boldsymbol{v}}{\partial t} + \int \mathrm{d}\nu \mu \frac{\partial f}{\partial t} \right) \\
&= \int \mathrm{d}\boldsymbol{x} \Bigg[\int \mathrm{d}\nu \mu L \cdot (D_0 \boldsymbol{I}^{-1} f L \mu) + \mu \nabla \cdot (\boldsymbol{J} f \nabla \mu) - \mu L \cdot (\boldsymbol{g} f) - \mu \nabla \cdot (\boldsymbol{v} f) \Bigg] \\
&- \rho_s \boldsymbol{v} \cdot (\boldsymbol{v} \cdot \nabla) \boldsymbol{v} - \boldsymbol{v} \cdot \nabla p + \boldsymbol{v} \cdot (\nabla \cdot \tau) + \boldsymbol{v} \cdot \boldsymbol{F}_e \\
&= \int \mathrm{d}\boldsymbol{x} \Bigg[\int \mathrm{d}\nu - f (L\mu)^T D_0 \boldsymbol{I}^{-1} (L\mu) - f (\nabla \mu)^T \boldsymbol{J} (\nabla \mu) + f \boldsymbol{g} \cdot L\mu + \boldsymbol{v} \cdot f \nabla \mu \Bigg] \\
&+ \frac{\rho_s}{2} (\nabla \cdot \boldsymbol{v}) |\boldsymbol{v}|^2 + p \nabla \cdot \boldsymbol{v} - \kappa : (\tau_e + \tau_f) + \boldsymbol{v} \cdot \boldsymbol{F}_e \\
&= \int \mathrm{d}\boldsymbol{x} \Bigg[\int \mathrm{d}\nu - f (L\mu)^T D_0 \boldsymbol{I}^{-1} (L\mu) - f (\nabla \mu)^T \boldsymbol{J} (\nabla \mu) \\
&+ (f \boldsymbol{g} \cdot L\mu - f (\kappa : \alpha_j) L_j \mu) + (\boldsymbol{v} \cdot f \nabla \mu - \boldsymbol{v} \cdot c\rho \nabla \mu)] - \kappa : \tau_f \\
&= \int \mathrm{d}\boldsymbol{x} \left[-\langle (L\mu)^T D_0 \boldsymbol{I}^{-1} (L\mu) \rangle - \langle (\nabla \mu)^T \boldsymbol{J} (\nabla \mu) \rangle - 2\eta \frac{\kappa + \kappa^T}{2} : \frac{\kappa + \kappa^T}{2} - \kappa : \tau_{vf} \right].
\end{aligned} \tag{2.33}$$

In the above, we ignore the boundary terms. Note that the first three terms are not positive. By (2.32) and (2.21) we know that the last term is not positive either.

2.3. Bent-core molecules and star molecules

For bent-core molecules and star molecules, the sphere centers are distributed in the plane $\widehat{O}\boldsymbol{m}_1\boldsymbol{m}_2$. In this case, we can simplify the expressions derived above. First, we have $I_{33} = I_{11} + I_{22}$. Thus, in (2.22),

$$\boldsymbol{g} = (\kappa : \boldsymbol{m}_2 \boldsymbol{m}_3) \boldsymbol{m}_1 - (\kappa : \boldsymbol{m}_1 \boldsymbol{m}_3) \boldsymbol{m}_2 + \frac{1}{I_{11} + I_{22}} (I_{22} \kappa : \boldsymbol{m}_1 \boldsymbol{m}_2 - I_{11} \kappa : \boldsymbol{m}_2 \boldsymbol{m}_1) \boldsymbol{m}_3. \tag{2.34}$$

Then in (2.29), we have

$$\alpha_1 = \boldsymbol{m}_2 \boldsymbol{m}_3, \ \alpha_2 = -\boldsymbol{m}_1 \boldsymbol{m}_3, \ \alpha_3 = \frac{1}{I_{11} + I_{22}} (I_{22} \boldsymbol{m}_1 \boldsymbol{m}_2 - I_{11} \boldsymbol{m}_2 \boldsymbol{m}_1). \tag{2.35}$$

By (2.21) and (2.32), we deduce that

$$\tau_{vf} = \frac{c\zeta\kappa}{m_0}:\Big[I_{22}\langle \boldsymbol{m}_1\boldsymbol{m}_1\boldsymbol{m}_1\boldsymbol{m}_1\rangle + I_{11}\langle \boldsymbol{m}_2\boldsymbol{m}_2\boldsymbol{m}_2\boldsymbol{m}_2\rangle + \frac{I_{11}I_{22}}{I_{11}+I_{22}}\langle(\boldsymbol{m}_1\boldsymbol{m}_2+\boldsymbol{m}_2\boldsymbol{m}_1)(\boldsymbol{m}_1\boldsymbol{m}_2+\boldsymbol{m}_2\boldsymbol{m}_1)\rangle\Big]. \tag{2.36}$$

We can see that the only difference in the above terms lies in the coefficients as functions of the moment of inertia, from which we can distinguish the bent-core molecules and star molecules. For a bent-core molecule (drawn in Fig. 1 left), the sphere centers are distributed uniformly and continuously on a two-segment broken line, where the length of each segment is $l/2$. Thus, $\hat{\rho}$ is given by

$$\hat{\rho}(\hat{\boldsymbol{r}}) = \frac{1}{l}\int_{-\frac{l}{2}}^{\frac{l}{2}} \mathrm{d}s\ \delta\left(\hat{\boldsymbol{r}} - \left(\frac{l}{4}-|s|\right)\cos\frac{\theta}{2}\boldsymbol{m}_1 - s\sin\frac{\theta}{2}\boldsymbol{m}_2\right). \tag{2.37}$$

Substituting it into (2.15) and recalling (2.16), we obtain

$$I_{11} = \frac{l^2 m_0}{48}\cdot 4\sin^2\frac{\theta}{2}, \quad I_{22} = \frac{l^2 m_0}{48}\cdot\cos^2\frac{\theta}{2}. \tag{2.38}$$

For a star molecule (drawn in Fig. 1 right), the sphere centers also lie in a third line segment of the length l_2. Thus, $\hat{\rho}$ is given by

$$\hat{\rho}(\hat{\boldsymbol{r}}) = \frac{1}{l+l_2}\left[\int_{-\frac{l}{2}}^{\frac{l}{2}} \mathrm{d}s\,\delta\left(\hat{\boldsymbol{r}} - (\frac{l}{4}-|s|)\cos\frac{\theta}{2}\boldsymbol{m}_1 - s\sin\frac{\theta}{2}\boldsymbol{m}_2\right) + \int_0^{l_2}\mathrm{d}s\,\delta(\hat{\boldsymbol{r}} - s\boldsymbol{m}_1)\right]. \tag{2.39}$$

Therefore,

$$I_{11} = \frac{l^2 m_0}{12}\sin^2\frac{\theta}{2}, \quad I_{22} = m_0\left(\frac{\frac{1}{3}l_2^3 + \frac{1}{12}l^3\cos^2\frac{\theta}{2}}{l+l_2} - x_C^2\right), \tag{2.40}$$

where

$$x_C = \frac{\frac{1}{2}l_2^2 - \frac{1}{4}l^2\cos\frac{\theta}{2}}{l+l_2}$$

is the $\boldsymbol{m}_1$-coordinate of the center of mass.

For bent-core molecules and star molecules, the spatial diffusion matrix $\boldsymbol{J}$ derived from the Kirkwood theory (see Appendix) is diagonal in the frame $(\boldsymbol{m}_i)$,

$$\boldsymbol{J} = \frac{1}{8\pi D\eta_0}\sum_{j=1}^{3}\gamma_j\boldsymbol{m}_j\boldsymbol{m}_j. \tag{2.41}$$

For bent-core molecules with $D/l = 1/40$, we plot γ in Fig. 2 right.

For the free energy, we adopt the tensor model derived in [42] from the second virial expansion with the hardcore molecular interaction. The hardcore interaction is determined only by the molecular shape, given by $\hat{\rho}$ in the current context. Assume that the concentration c is constant. Define $\boldsymbol{p} = \langle \boldsymbol{m}_1\rangle$, $Q_1 = \langle \boldsymbol{m}_1\boldsymbol{m}_1\rangle$, $Q_2 = \langle \boldsymbol{m}_2\boldsymbol{m}_2\rangle$. For both molecules, F_r shares the form below,

$$\begin{aligned}\frac{F_r}{k_BT} = \int \mathrm{d}\boldsymbol{x}\,\frac{c^2}{2}\Big(&c_{01}|\boldsymbol{p}|^2 + c_{02}\left|Q_1\right|^2 + c_{03}\left|Q_2\right|^2 + 2c_{04}Q_1{:}\,Q_2)\\ &+c^2(c_{11}p_j\partial_i Q_{1ij} + c_{12}p_j\partial_i Q_{2ij})\\ &+\frac{c^2}{4}[c_{21}|\nabla\boldsymbol{p}|^2 + c_{22}|\nabla Q_1|^2 + c_{23}|\nabla Q_2|^2 + 2c_{24}\partial_i Q_{1jk}\partial_i Q_{2jk}\\ &+2c_{27}\partial_i p_i\partial_j p_j + 2c_{28}\partial_i Q_{1ik}\partial_j Q_{1jk} + 2c_{29}\partial_i Q_{2ik}\partial_j Q_{2jk} + 4c_{2,10}\partial_i Q_{1ik}\partial_j Q_{2jk}],\end{aligned} \tag{2.42}$$

which is determined by the molecular symmetry [42,43]. The difference also lies in the coefficients c_{kj}. They are derived as functions of the molecular parameters l, D, θ for bent-core molecules, and also l_2 for star molecules. They possess the scaling property

$$c_{kj} = l^{k+3}\tilde{c}_{kj}(D/l,\ \theta,\ l_2/l). \tag{2.43}$$

The calculation of c_{kj} is discussed in [42,43]. In Fig. 2 left we plot c_{02}, c_{03}, c_{04} that are necessary for the shear flow problem. With F_r given, $\boldsymbol{F}_e$ and τ_e are determined by (2.27) and (2.29).

To summarize, we establish the dynamic model from the molecular shape described by $\hat{\rho}$, and the free energy $F[f]$. In the case of hardcore interaction, $F[f]$ is also determined by the molecular shape. Therefore, the model is able to characterize the dynamics of molecules with different shapes. In particular, for bent-core molecules and star molecules, the model has the same form, no matter for the free energy F and other terms. The two types of molecules are distinguished by numerous coefficients in the model, which are expressed as functions of molecular parameters.

3. Tensor model

We derive the tensor model from the molecular model. When we use the free energy (2.42), the elastic stress τ_e and the external force $\boldsymbol{F}_e$ can also be expressed by tensors. Let V be computed from the free energy (2.42). Denote

$$V_{\boldsymbol{p}} = \frac{1}{k_BT}\cdot\frac{\delta F_r}{\delta \boldsymbol{p}},\quad V_{Q_1} = \frac{1}{k_BT}\cdot\frac{\delta F_r}{\delta Q_1},\quad V_{Q_2} = \frac{1}{k_BT}\cdot\frac{\delta F_r}{\delta Q_2}.$$

Direct computation gives

$$V_{\boldsymbol{p}} = c_{01}\boldsymbol{p} + c_{11}\nabla\cdot Q_1 + c_{12}\nabla\cdot Q_2 - c_{21}\Delta\boldsymbol{p} - c_{27}\nabla(\nabla\cdot\boldsymbol{p}), \tag{3.1}$$

$$V_{Q_1} = c_{02}Q_1 + c_{04}Q_2 - c_{11}\nabla\boldsymbol{p} - c_{22}\Delta Q_1 - c_{24}\Delta Q_2 - c_{28}\nabla(\nabla\cdot Q_1) - c_{2,10}\nabla(\nabla\cdot Q_2), \tag{3.2}$$

$$V_{Q_2} = c_{04}Q_1 + c_{03}Q_2 - c_{12}\nabla\boldsymbol{p} - c_{24}\Delta Q_1 - c_{23}\Delta Q_2 - c_{2,10}\nabla(\nabla\cdot Q_1) - c_{29}\nabla(\nabla\cdot Q_2). \tag{3.3}$$

And we can verify that $V = \delta F_r/\delta f$ satisfies

$$V = V_{\boldsymbol{p}}\cdot\boldsymbol{m}_1 + V_{Q_1}{:}\,\boldsymbol{m}_1\boldsymbol{m}_1 + V_{Q_2}{:}\,\boldsymbol{m}_2\boldsymbol{m}_2. \tag{3.4}$$

Thus

$$L_iV = V_{\boldsymbol{p}}\cdot(L_i\boldsymbol{m}_1) + V_{Q_1}{:}\,(L_i\boldsymbol{m}_1\boldsymbol{m}_1) + V_{Q_2}{:}\,(L_i\boldsymbol{m}_2\boldsymbol{m}_2). \tag{3.5}$$

From this equation, the elastic stress can be written as

$$\begin{aligned}\tau_e = ck_BT\{&\langle \boldsymbol{m}_2\boldsymbol{m}_2 - \boldsymbol{m}_3\boldsymbol{m}_3\rangle + V_{Q_2}{:}\,\langle(\boldsymbol{m}_2\boldsymbol{m}_3+\boldsymbol{m}_3\boldsymbol{m}_2)\boldsymbol{m}_2\boldsymbol{m}_3\rangle\\ &+\langle \boldsymbol{m}_1\boldsymbol{m}_1 - \boldsymbol{m}_3\boldsymbol{m}_3\rangle + V_{\boldsymbol{p}}\cdot\langle \boldsymbol{m}_3\boldsymbol{m}_1\boldsymbol{m}_3\rangle + V_{Q_1}{:}\,\langle(\boldsymbol{m}_1\boldsymbol{m}_3+\boldsymbol{m}_3\boldsymbol{m}_1)\boldsymbol{m}_1\boldsymbol{m}_3\rangle\\ &+\frac{1}{I_{11}+I_{22}}\Big[(I_{22}-I_{11})\langle \boldsymbol{m}_2\boldsymbol{m}_2 - \boldsymbol{m}_1\boldsymbol{m}_1\rangle + V_{\boldsymbol{p}}\cdot\langle \boldsymbol{m}_2(I_{22}\boldsymbol{m}_1\boldsymbol{m}_2 - I_{11}\boldsymbol{m}_2\boldsymbol{m}_1)\rangle\\ &+(V_{Q_1}-V_{Q_2}){:}\,\langle(\boldsymbol{m}_1\boldsymbol{m}_2+\boldsymbol{m}_2\boldsymbol{m}_1)(I_{22}\boldsymbol{m}_1\boldsymbol{m}_2 - I_{11}\boldsymbol{m}_2\boldsymbol{m}_1)\rangle\Big]\}.\end{aligned} \tag{3.6}$$

And the external force is written as

$$\boldsymbol{F}_e = -ck_BT\nabla(V_{\boldsymbol{p}}\cdot\boldsymbol{p} + V_{Q_1}{:}\,Q_1 + V_{Q_2}{:}\,Q_2). \tag{3.7}$$

Now the Eq. (2.26) is only relevant to the tensors. For the Eq. (2.24), we multiply it by the tensors and integrate in SO_3. Generally, we can write

$$\frac{\partial A}{\partial t} + \boldsymbol{v}\cdot\nabla A = \mathscr{N}_A + \mathscr{M}_A + \mathscr{V}_A, \tag{3.8}$$

where A is arbitrary tensor, and $\mathscr{N}_A$, $\mathscr{M}_A$, $\mathscr{V}_A$ are the terms computed from spatial diffusion terms, rotational diffusion terms, and rotational convection terms. We need the integration by parts (2.9) and (2.8) when computing these terms. Take Q_1 as an example. After multiplying $\boldsymbol{m}_1\boldsymbol{m}_1$ and doing the integration, the following term appears,

$$\begin{aligned}\int \mathrm{d}\nu\boldsymbol{m}_1\boldsymbol{m}_1D_2L_2^2f &= D_2\int \mathrm{d}\nu L_2^2(\boldsymbol{m}_1\boldsymbol{m}_1)f\\ &= D_2\int \mathrm{d}\nu 2(\boldsymbol{m}_3\boldsymbol{m}_3 - \boldsymbol{m}_1\boldsymbol{m}_1)f = 2D_2\langle \boldsymbol{m}_3\boldsymbol{m}_3 - \boldsymbol{m}_1\boldsymbol{m}_1\rangle.\end{aligned} \tag{3.9}$$

Similarly, we can derive that

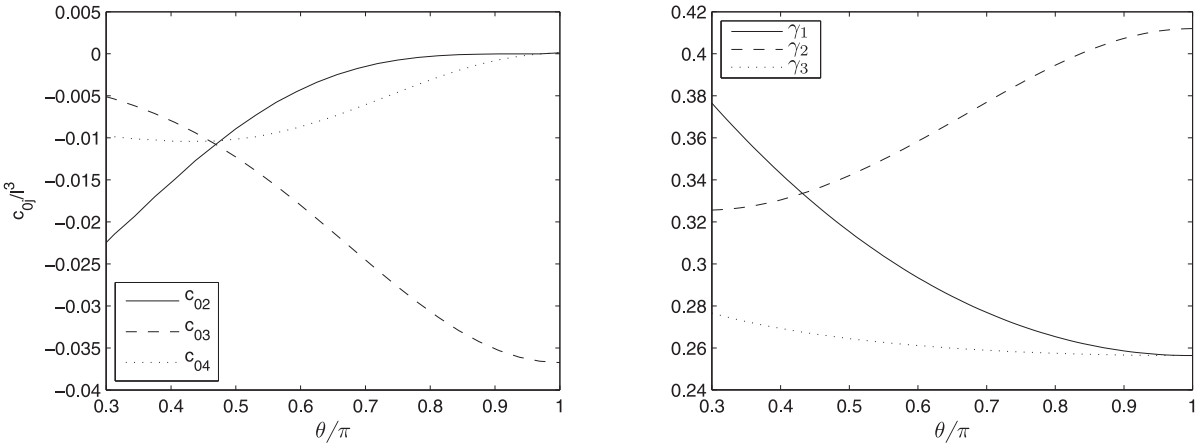

Fig. 2. Some coefficients in the model for bent-core molecules with $D/l = 1/40$. Left: coefficients of the bulk energy. Right: translational diffusion coefficients.

$$
\begin{aligned}
-\mathscr{M}_{\boldsymbol{p}} \;=\;& D_2[\boldsymbol{p} + V_{\boldsymbol{p}}\cdot\langle \boldsymbol{m}_3\boldsymbol{m}_3\rangle + V_{Q_1}\colon(\langle \boldsymbol{m}_1\boldsymbol{m}_3\boldsymbol{m}_3\rangle + \langle \boldsymbol{m}_3\boldsymbol{m}_1\boldsymbol{m}_3\rangle)]\\
&+ D_3[\boldsymbol{p} + V_{\boldsymbol{p}}\cdot\langle \boldsymbol{m}_2\boldsymbol{m}_2\rangle + (V_{Q_1} - V_{Q_2})\colon(\langle \boldsymbol{m}_1\boldsymbol{m}_2\boldsymbol{m}_2\rangle + \langle \boldsymbol{m}_2\boldsymbol{m}_1\boldsymbol{m}_2\rangle)].
\end{aligned}
\tag{3.10}
$$

$$
\begin{aligned}
-\mathscr{M}_{Q_1} \;=\;& D_2[2(Q_1 - Q_3) + V_{\boldsymbol{p}}\cdot(\langle \boldsymbol{m}_3\boldsymbol{m}_3\boldsymbol{m}_1\rangle + \langle \boldsymbol{m}_3\boldsymbol{m}_1\boldsymbol{m}_3\rangle)\\
&+ V_{Q_1}\colon\langle(\boldsymbol{m}_1\boldsymbol{m}_3 + \boldsymbol{m}_3\boldsymbol{m}_1)(\boldsymbol{m}_1\boldsymbol{m}_3 + \boldsymbol{m}_3\boldsymbol{m}_1)\rangle]\\
&+ D_3[2(Q_1 - Q_2) + V_{\boldsymbol{p}}\cdot(\langle \boldsymbol{m}_2\boldsymbol{m}_2\boldsymbol{m}_1\rangle + \langle \boldsymbol{m}_2\boldsymbol{m}_1\boldsymbol{m}_2\rangle)\\
&+ (V_{Q_1} - V_{Q_2})\colon\langle(\boldsymbol{m}_1\boldsymbol{m}_2 + \boldsymbol{m}_2\boldsymbol{m}_1)(\boldsymbol{m}_1\boldsymbol{m}_2 + \boldsymbol{m}_2\boldsymbol{m}_1)\rangle].
\end{aligned}
\tag{3.11}
$$

$$
\begin{aligned}
-\mathscr{M}_{Q_2} \;=\;& D_1[2(Q_2 - Q_3) + V_{Q_2}\colon\langle(\boldsymbol{m}_2\boldsymbol{m}_3 + \boldsymbol{m}_3\boldsymbol{m}_2)(\boldsymbol{m}_2\boldsymbol{m}_3 + \boldsymbol{m}_3\boldsymbol{m}_2)\rangle]\\
&+ D_3[2(Q_2 - Q_1) - V_{\boldsymbol{p}}\cdot(\langle \boldsymbol{m}_2\boldsymbol{m}_2\boldsymbol{m}_1\rangle + \langle \boldsymbol{m}_2\boldsymbol{m}_1\boldsymbol{m}_2\rangle)\\
&- (V_{Q_1} - V_{Q_2})\colon\langle(\boldsymbol{m}_1\boldsymbol{m}_2 + \boldsymbol{m}_2\boldsymbol{m}_1)(\boldsymbol{m}_1\boldsymbol{m}_2 + \boldsymbol{m}_2\boldsymbol{m}_1)\rangle].
\end{aligned}
\tag{3.12}
$$

$$
\mathscr{V}_{\boldsymbol{p}} \;=\; \kappa\colon\left[\langle \boldsymbol{m}_1\boldsymbol{m}_3\boldsymbol{m}_3\rangle + \frac{I_{22}}{I_{11}+I_{22}}\langle \boldsymbol{m}_1\boldsymbol{m}_2\boldsymbol{m}_2\rangle - \frac{I_{11}}{I_{11}+I_{22}}\langle \boldsymbol{m}_2\boldsymbol{m}_1\boldsymbol{m}_2\rangle\right].
\tag{3.13}
$$

$$
\begin{aligned}
\mathscr{V}_{Q_1} \;=\;& \kappa\colon\left[\langle \boldsymbol{m}_1\boldsymbol{m}_3(\boldsymbol{m}_1\boldsymbol{m}_3 + \boldsymbol{m}_3\boldsymbol{m}_1)\rangle + \frac{I_{22}}{I_{11}+I_{22}}\langle \boldsymbol{m}_1\boldsymbol{m}_2(\boldsymbol{m}_1\boldsymbol{m}_2 + \boldsymbol{m}_2\boldsymbol{m}_1)\rangle\right.\\
&\left. - \frac{I_{11}}{I_{11}+I_{22}}\langle \boldsymbol{m}_2\boldsymbol{m}_1(\boldsymbol{m}_1\boldsymbol{m}_2 + \boldsymbol{m}_2\boldsymbol{m}_1)\rangle\right].
\end{aligned}
\tag{3.14}
$$

$$
\begin{aligned}
\mathscr{V}_{Q_2} \;=\;& \kappa\colon\left[\langle \boldsymbol{m}_2\boldsymbol{m}_3(\boldsymbol{m}_2\boldsymbol{m}_3 + \boldsymbol{m}_3\boldsymbol{m}_2)\rangle - \frac{I_{22}}{I_{11}+I_{22}}\langle \boldsymbol{m}_1\boldsymbol{m}_2(\boldsymbol{m}_1\boldsymbol{m}_2 + \boldsymbol{m}_2\boldsymbol{m}_1)\rangle\right.\\
&\left. + \frac{I_{11}}{I_{11}+I_{22}}\langle \boldsymbol{m}_2\boldsymbol{m}_1(\boldsymbol{m}_1\boldsymbol{m}_2 + \boldsymbol{m}_2\boldsymbol{m}_1)\rangle\right].
\end{aligned}
\tag{3.15}
$$

$$
\begin{aligned}
(\mathscr{N}_{\boldsymbol{p}})_\alpha =\;& \partial_i\left(\partial_j\sum_{\sigma=1}^{3}\gamma_\sigma\langle m_{1\alpha}m_{\sigma i}m_{\sigma j}\rangle + \partial_j(V_{\boldsymbol{p}})_k\sum_{\sigma=1}^{3}\gamma_\sigma\langle m_{1k}m_{1\alpha}m_{\sigma i}m_{\sigma j}\rangle\right.\\
&+ \partial_j(V_{Q_1})_{kl}\sum_{\sigma=1}^{3}\gamma_\sigma\langle m_{1k}m_{1l}m_{1\alpha}m_{\sigma i}m_{\sigma j}\rangle\\
&\left.+ \partial_j(V_{Q_2})_{kl}\sum_{\sigma=1}^{3}\gamma_\sigma\langle m_{2k}m_{2l}m_{1\alpha}m_{\sigma i}m_{\sigma j}\rangle\right).
\end{aligned}
\tag{3.16}
$$

$$
\begin{aligned}
(\mathscr{N}_{Q_1})_{\alpha\beta} \;=\;& \partial_i\left(\partial_j\sum_{\sigma=1}^{3}\gamma_\sigma\langle m_{1\alpha}m_{1\beta}m_{\sigma i}m_{\sigma j}\rangle + \partial_j(V_{\boldsymbol{p}})_k\sum_{\sigma=1}^{3}\gamma_\sigma\langle m_{1k}m_{1\alpha}m_{1\beta}m_{\sigma i}m_{\sigma j}\rangle\right.\\
&+ \partial_j(V_{Q_1})_{kl}\sum_{\sigma=1}^{3}\gamma_\sigma\langle m_{1k}m_{1l}m_{1\alpha}m_{1\beta}m_{\sigma i}m_{\sigma j}\rangle\\
&\left.+ \partial_j(V_{Q_2})_{kl}\sum_{\sigma=1}^{3}\gamma_\sigma\langle m_{2k}m_{2l}m_{1\alpha}m_{1\beta}m_{\sigma i}m_{\sigma j}\rangle\right).
\end{aligned}
\tag{3.17}
$$

$$
\begin{aligned}
(\mathscr{N}_{Q_2})_{\alpha\beta} \;=\;& \partial_i\left(\partial_j\sum_{\sigma=1}^{3}\gamma_\sigma\langle m_{2\alpha}m_{2\beta}m_{\sigma i}m_{\sigma j}\rangle + \partial_j(V_{\boldsymbol{p}})_k\sum_{\sigma=1}^{3}\gamma_\sigma\langle m_{1k}m_{2\alpha}m_{2\beta}m_{\sigma i}m_{\sigma j}\rangle\right.\\
&+ \partial_j(V_{Q_1})_{kl}\sum_{\sigma=1}^{3}\gamma_\sigma\langle m_{1k}m_{1l}m_{2\alpha}m_{2\beta}m_{\sigma i}m_{\sigma j}\rangle\\
&\left.+ \partial_j(V_{Q_2})_{kl}\sum_{\sigma=1}^{3}\gamma_\sigma\langle m_{2k}m_{2l}m_{2\alpha}m_{2\beta}m_{\sigma i}m_{\sigma j}\rangle\right).
\end{aligned}
\tag{3.18}
$$

To make the equations form a closed system, we need to express high-order tensors as functions of ($\boldsymbol{p}$, Q_1, Q_2). Here we use the quasi-equilibrium approximation, namely to choose f that minimizes the entropy term $\int \mathrm{d}\nu f\log f$ with ($\boldsymbol{p}$, Q_1, Q_2) equal to the given value. Remember that $f = c\rho$ where c is constant. Thus ρ is given by [42]

$$
\rho(P) = \frac{1}{Z}\exp(\boldsymbol{b}\cdot\boldsymbol{m}_1 + B_1\colon \boldsymbol{m}_1\boldsymbol{m}_1 + B_2\colon \boldsymbol{m}_2\boldsymbol{m}_2),
\tag{3.19}
$$

where $\boldsymbol{b}$ is a vector, B_1 and B_2 are symmetric matrices, and

$$
Z = \int \mathrm{d}\nu\exp\left(\boldsymbol{b}\cdot\boldsymbol{m}_1 + B_1\colon \boldsymbol{m}_1\boldsymbol{m}_1 + B_2\colon \boldsymbol{m}_2\boldsymbol{m}_2\right).
\tag{3.20}
$$

Now the system is described by ($\boldsymbol{p}$, Q_1, Q_2). The evolution of three tensors is governed by (3.8) in which the terms are given by (3.10)–(3.18), together with (2.25) and (2.26) in which the terms are given by (2.36), (3.6), (3.7). The high-order tensors are computed from (3.19), which keeps f positive and the energy dissipation law. It is obvious that f is positive, and we can deduce that

$$\begin{aligned}&\frac{\mathrm{d}}{\mathrm{d}t}\left(F[\boldsymbol{p}, Q_1, Q_2] + \int \mathrm{d}\boldsymbol{x}\frac{\rho|\boldsymbol{v}|^2}{2}\right)\\&= \int \mathrm{d}\boldsymbol{x}\{-ck_BT[D_1\langle(\mu_{Q_2}\colon(\boldsymbol{m}_2\boldsymbol{m}_3+\boldsymbol{m}_3\boldsymbol{m}_2))^2\rangle\\&+D_2\langle(\mu_{\boldsymbol{p}}\cdot\boldsymbol{m}_3+\mu_{Q_1}\colon(\boldsymbol{m}_2\boldsymbol{m}_3+\boldsymbol{m}_3\boldsymbol{m}_2))^2\rangle\\&+D_3\langle(\mu_{\boldsymbol{p}}\cdot\boldsymbol{m}_2+(\mu_{Q_1}-\mu_{Q_2})\colon(\boldsymbol{m}_2\boldsymbol{m}_3+\boldsymbol{m}_3\boldsymbol{m}_2))^2\rangle]\\&-ck_BT\sum_{\sigma=1}^{3}\gamma_\sigma\langle[\partial_j(\mu_{\boldsymbol{p}})_k m_{1k}m_{\sigma j}+\partial_j(\mu_{Q_1})_{kl}m_{1k}m_{1l}m_{\sigma j}+\partial_j(\mu_{Q_2})_{kl}m_{2k}m_{2l}m_{\sigma j}]^2\rangle\\&-2\eta\frac{\kappa+\kappa^T}{2}\colon\frac{\kappa+\kappa^T}{2}-c\zeta[I_{22}\langle(\kappa\colon\boldsymbol{m}_1\boldsymbol{m}_1)^2\rangle+I_{11}\langle(\kappa\colon\boldsymbol{m}_2\boldsymbol{m}_2)^2\rangle\\&+\frac{I_{11}I_{22}}{I_{11}+I_{22}}\langle(\kappa\colon(\boldsymbol{m}_1\boldsymbol{m}_2+\boldsymbol{m}_2\boldsymbol{m}_1))^2\rangle]\Big\}.\end{aligned} \tag{3.21}$$

In the above, we denote $\mu_{\boldsymbol{p}} = \delta F/\delta\boldsymbol{p}$, etc. The details are given in Appendix. Note that each of the right-hand terms is not positive. We point out that the form of the tensor model is also determined by molecular symmetry, and the coefficients are functions of molecular parameters.

4. Numerical results

In this section, we focus on the shear flow problem. We assume that the velocity is along the x-direction, and the gradient is along the y-direction, and

$$\kappa_{12} = \partial_2 v_1 = k$$

is a constant. We also assume that the tensors are spatially homogeneous. Thus, we only need the bulk energy in (2.42) and will discard the gradient terms. In this case, the equation of momentum holds naturally, and we need to solve the Smoluchowski equation only.

We rescale the time unit by $\tilde{t} = (\zeta l^2/48k_BT)^{-1}t$. It cancels the k_BT in the free energy and the units in the rotational diffusion coefficients D_i. For bent-core molecules, the rescaling let

$$(D_1^{-1}, D_2^{-1}, D_3^{-1}) = \left(4\sin^2\frac{\theta}{2}, \cos^2\frac{\theta}{2}, 1+3\sin^2\frac{\theta}{2}\right).$$

After the rescaling, the shear rate k becomes dimensionless. In the free energy, by (2.43) we rescale $\tilde{\boldsymbol{x}} = \boldsymbol{x}/l$ and reduce the shape parameters to three dimensionless ones: $\eta = D/l$, l_2/l, and θ. We fix $\eta = 1/40$, and express the concentration by $\alpha = cD^2(l+l_2)$ that is proportional to the volume fraction $(\pi/4)cD^2(l+l_2)$.

In what follows, we examine both the molecular model and the tensor model, and compare the flowing modes shown by both models.

4.1. Numerical method

For the tensor model, we use (3.19) to convert the equations of tensors into equations of $(\boldsymbol{b}, B_1, B_2)$,

$$\frac{\mathrm{d}(\boldsymbol{b}, B_1, B_2)}{\mathrm{d}t} = \left(\frac{\partial(\boldsymbol{p}, Q_1, Q_2)}{\partial(\boldsymbol{b}, B_1, B_2)}\right)^{-1}\frac{\mathrm{d}(\boldsymbol{p}, Q_1, Q_2)}{\mathrm{d}t}. \tag{4.1}$$

The derivatives $\frac{\partial(\boldsymbol{p}, Q_1, Q_2)}{\partial(\boldsymbol{b}, B_1, B_2)}$ are computed by (A.4). They are expressed by high-order tensors. The tensors are computed by numerical integration about the Euler angles. Each of the Euler angles is discretized by 32 points. The time discretization is implemented by the classical fourth-order Runge–Kutta method with the time step $\delta t = 10^{-2}$. The initial value is chosen as $B_1 = B_2 = 0$, while $\boldsymbol{b} = (1.4, 2.8, 1.4)^T$ pointing to a tilted direction.

For the molecular model, we adopt a spectral-Galerkin method, where we use Wigner D-matrix $D^j_{mm'}$ (see, for example, [41]), truncated at $j \le 10$, to discretize the density function f. For the time integration, we also use the classical fourth-order Runge–Kutta method, with the time step $\delta t = 5\times10^{-3}$. For the initial value, we start from the Boltzmann distribution with $B_1 = B_2 = 0$ and $\boldsymbol{b} = (1.4, 2.8, 1.4)^T$. We let it evolve 2000 time steps under the parameter $\alpha = 0.5$, $\theta = 23\pi/32$, $k = 6.4$, and take the result as the initial value.

4.2. Flow modes

Before looking at the flow modes, we review the homogeneous nematic phases shown by bent-core molecules and star molecules in quiescent fluid, namely $k = 0$, which are discussed in [42]. In these phases we have $\boldsymbol{p} = 0$. Denote $Q_3 = \langle\boldsymbol{m}_3\boldsymbol{m}_3\rangle = I - Q_1 - Q_2$. Bent-core molecules and star molecules can exhibit the uniaxial nematic phase, where we can find a unit vector $\boldsymbol{n}$ such that

$$Q_i = s_i\left(\boldsymbol{n}\boldsymbol{n} - \frac{I}{3}\right) + \frac{I}{3}, \quad i = 1, 2, 3.$$

According to the signs of s_i, the uniaxial nematic phase is further classified. It is the N_2 phase where $s_1, s_3 < 0$, $s_2 > 0$, indicating that $\boldsymbol{m}_2$ accumulates near $\boldsymbol{n}$ and $\boldsymbol{m}_1$, $\boldsymbol{m}_3$ accumulate near the plane vertical to $\boldsymbol{n}$; and the N_3 phase where $s_1, s_2 < 0$, $s_3 > 0$, indicating that $\boldsymbol{m}_3$ accumulates near $\boldsymbol{n}$ and $\boldsymbol{m}_2$, $\boldsymbol{m}_3$ accumulate near the plane vertical to $\boldsymbol{n}$. We can also observe the biaxial nematic phase (B), where we can find an orthonormal frame $(\boldsymbol{n}_1, \boldsymbol{n}_2, \boldsymbol{n}_3)$ such that

$$Q_i = s_{i1}\boldsymbol{n}_1\boldsymbol{n}_1 + s_{i2}\boldsymbol{n}_2\boldsymbol{n}_2 + s_{i3}\boldsymbol{n}_3\boldsymbol{n}_3.$$

The eigenvalues satisfy $s_{ii} > s_{ij}\,(j \ne i)$, indicating that $\boldsymbol{m}_i$ is preferably along $\boldsymbol{n}_i$.

Both bent-core molecules and star molecules exhibit the isotropic phase with small α, and the modulated twist-bend phase with large α. Thus, in this work we will choose intermediate α to let the system have homogeneous nematic phases in equilibrium. For bent-core molecules, we choose $\alpha = 0.42$, 0.5, and examine the bending angles $\theta = j\pi/32$ where $16 \le j \le 23$. For both α, it shows the N_2 phase for $20 \le j \le 23$, the N_3 phase for $16 \le j \le 18$, and the B phase for $j = 19$. For star molecules, we fix $\alpha = 0.42$, $\theta = 2\pi/3$ and examine $l_2/l = j/40$ where $5 \le j \le 11$. It shows the N_2 phase when $j = 5$, the N_3 phase when $j = 11$, and the B phase when $6 \le j \le 10$.

We choose the shear rates as $k = 0.2n$, $n = 1, \ldots, 100$. Since $\boldsymbol{p}$ is zero in quiescent fluid, we are interested in whether $\boldsymbol{p}$ appears. Actually, under our choice of parameters, $|\boldsymbol{p}|$ always decays rapidly. In equilibrium, it results from $c_{01} > 0$ for the hardcore molecular interaction (see [43]). The results in dynamics suggest that in homogeneous flow $\boldsymbol{p}$ will not be induced. In the following, we no longer look at $\boldsymbol{p}$ and focus on Q_1 and Q_2. Denote the unit eigenvector of the largest eigenvalue of Q_i as $\boldsymbol{q}_i$ for $i = 1, 2$. Note that in quiescent fluid $\boldsymbol{q}_1$ and $\boldsymbol{q}_2$ are vertical. Although it does not hold in shear flow, we find that $\boldsymbol{q}_1$ and $\boldsymbol{q}_2$ are always approximately vertical. Actually, in most cases, we have $\cos\langle\boldsymbol{q}_1, \boldsymbol{q}_2\rangle \le 0.1$. This value may become a little larger when the shear rate k is near the transition value between two flow modes. At that time, the largest and second eigenvalues of Q_1 or Q_2 might be very close so that $\boldsymbol{q}_1$ and $\boldsymbol{q}_2$ are sensitive to the value of Q_1 and Q_2. Thus, we may view the molecule as having a preferred orientation such that $\boldsymbol{m}_i$ is near $\boldsymbol{q}_i$, and classify the flow modes according to the motion of $\boldsymbol{q}_i$.

4.2.1. Molecular model

For the molecular model, the flow modes are described below.

1. Log-rolling (LR): steady state, where $\boldsymbol{q}_2$ is along the z- (vortex) direction, and $\boldsymbol{q}_1$ lies in the $x-y$ (shear) plane.
2. Kayaking(K): one of $\boldsymbol{q}_1$ and $\boldsymbol{q}_2$ rotates round the z-axis, while the other shows a splayed pattern (see Fig. 4 left). If $\boldsymbol{q}_i$ rotates round the z-axis, we denote the flow mode as K-Q_i.

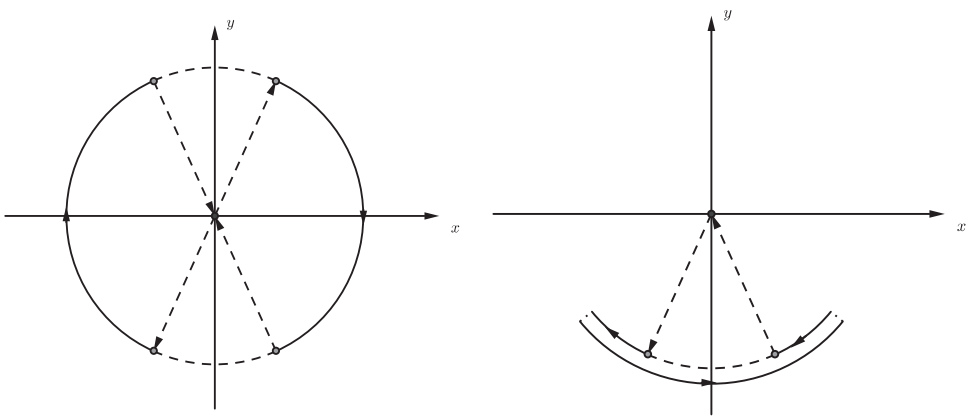

Fig. 3. Left: Tumbling motion of $\boldsymbol{q}_1$. Right: Wagging-alternating motion of $\boldsymbol{q}_1$.

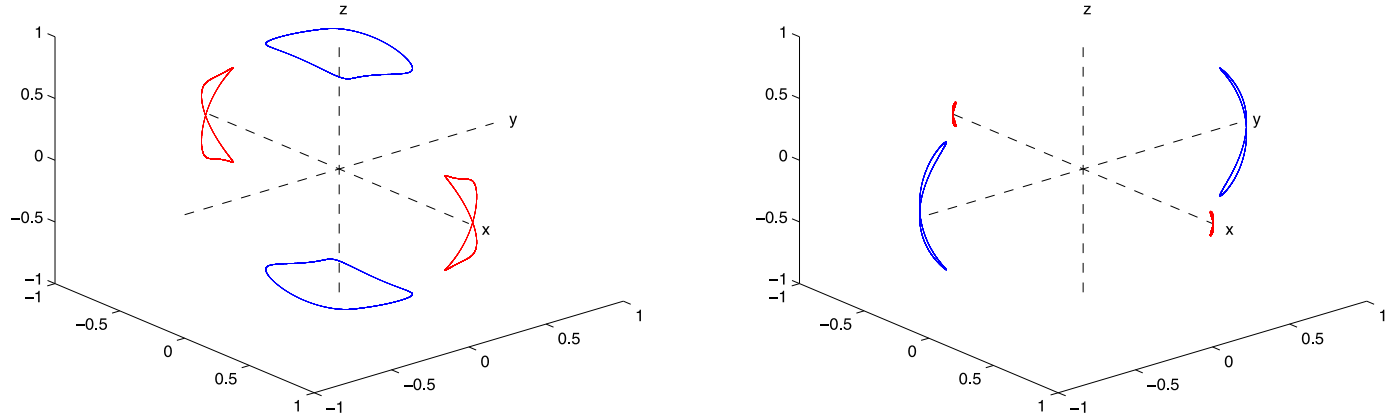

Fig. 4. Left: Kayaking. The red and blue lines are motions of $\pm\ \boldsymbol{q}_1$ and $\pm\ \boldsymbol{q}_2$: when $\boldsymbol{q}_1$ corresponds to blue line, it shows K-Q_1 mode; otherwise it shows K-Q_2 mode. Right: Double splayed, where red line gives the motion of $\pm\ \boldsymbol{q}_2$, and blue line gives the motions of $\pm\ \boldsymbol{q}_1$. (For interpretation of the references to colour in this figure legend, the reader is referred to the web version of this article.)

3. Double splayed (DS): $\boldsymbol{q}_2$ shows splayed pattern near the x-axis, $\boldsymbol{q}_1$ shows splayed near the y-axis (see Fig. 4 right).
4. Tumbling (T): $\boldsymbol{q}_2$ rotates in the $x-y$ plane; $\boldsymbol{q}_1$ also rotates in the plane, but jumps to z when it approaches the y axis (see Fig. 3 left).
5. Wagging: $\boldsymbol{q}_2$ shows wagging near the x-axis. According to the motion of $\boldsymbol{q}_1$, it is further classified into two cases.
   - Wagging-alternating (W-A): $\boldsymbol{q}_1$ is wagging near the y-axis, with a jump to the z-axis (see Fig. 3 right).
   - Wagging-wagging (W-W): $\boldsymbol{q}_1$ is wagging near the y-axis.
6. Flow-aligning (FA): steady state, where $\boldsymbol{q}_2$ lies in the $x-y$ plane, while $\boldsymbol{q}_1$ may be in the $x-y$ plane (FA-y) or along the z axis (FA-z).

First we examine the flow modes for bent-core molecules. The range of shear rates for each flow mode in molecular model is listed in Table 1a and b. For $\theta = 19\pi/32$ and $\alpha = 0.5$, the flow modes are

K-Q_2: [0, 2.8], K-Q_1: [3.0, 6.8], FA-z: [7.0, 20.0].

We have mentioned that in quiescent fluid, the bending angle $\theta = j\pi/32$ determines which of the three nematic phase is observed. In shear flow, different nematic phases result in distinct flow mode sequences with the shear rate k increasing. When $16 \le j \le 18$, namely the equilibrium phase is N_3, the only flow mode is FA-z. When $j = 19$, namely the equilibrium phase is B, we obtain only FA-z for $\alpha = 0.42$, and the K-Q_2 — K-Q_1 — FA-z sequence for $\alpha = 0.5$. When $20 \le j \le 23$, namely the equilibrium phase is N_2, the sequence follows LR — K-Q_2 — T — W-A — W-W — FA-y — FA-z, with one or two modes missing. For $\alpha = 0.42$, T is missing for all the four angles, and LR is not shown for $j = 20$. For $\alpha = 0.5$, LR is not found for $j = 23$, K-Q_2 is not shown for $j = 21$, T and W-A are missing for $j = 20$, and FA-z is not exhibited for $j = 22, 23$.

For star molecules, we can have a closer look at the effect of molecular shape in the biaxial region (Table 2). Recall that as l_2/l increases, the equilibrium phase sequence is N_2 — B — N_3. At $l_2/l = 0.125$, the flow mode sequence is LR — K-Q_2 — W-W — FA-y — FA-z, which is part of the sequence found for bent-core molecules in the N_2 region. When l_2/l increases and enters the B region, the K-Q_1 mode emerges between FA-y and FA-z. Then we observe some subtle phenomena when l_2/l further increases. At $l_2/l = 0.2$, the K-Q_2 mode moves to the middle of FA-y and K-Q_1. At $l_2/l = 0.225$, the mode at low shear rates changes from LR to K-Q_2 and LR emerges at high shear rates, resulting in the sequence K-Q_2 — W-W — FA-y — K-Q_2 — LR — FA-z. Then at $l_2/l = 0.25$, K-Q_2 at high shear rates vanishes. Finally at $l_2/l = 0.275$, the two periodic modes K-Q_2 and W-W are substituted by DS.

Because rod-like molecules also show the N_2 phase in equilibrium, we would like to compare the flow modes of bent-core molecules with $\theta = j\pi/32$, $20 \le j \le 23$ with those of rod-like molecules that have been studied extensively in literature. If we only look at the motion of $\boldsymbol{q}_2$, the five modes are also found for rod-like molecules. The out-of-plane steady and out-of-plane oscillating states are also exhibited by rod-like molecules but are not shown in our results. The works on rod-like molecules imply that the occurrence of two out-of-plane modes might require a careful choice of α near the isotropic-nematic transition (see the solution diagrams in [12]). Our choice of α, however, is

Table 1
Range of the shear rate k for flow modes in the molecular model for bent-core molecules.

θ	LR	K-Q_2	T	W-A	W-W	FA-y	FA-z
23π/32	–	[0, 10.0]	[10.2, 12.0]	[12.2, 14.8]	[15.0, 17.0]	[17.2, 20.0]	–
22π/32	[0.2, 7.0]	[7.2, 8.6]	[8.8, 9.4]	[9.6, 12.0]	[12.2, 13.6]	[13.8, 20.0]	–
21π/32	[0.2, 5.6]	–	[5.8, 6.0]	[6.2, 8.0]	[8.2, 9.6]	[9.8, 16.2]	[16.4, 20.0]
20π/32	[0.2, 2.8]	[3.0, 3.4]	–	–	[3.6, 5.2]	[5.4, 11.0]	[11.2, 20.0]
18π/32	–	–	–	–	–	–	[0.2, 20.0]
17π/32	–	–	–	–	–	–	[0.2, 20.0]
16π/32	–	–	–	–	–	–	[0.2, 20.0]

(a) $\alpha = 0.5$.

θ	LR	K-Q_2	T	W-A	W-W	FA-y	FA-z
23π/32	[0.2, 9.0]	[9.2, 9.4]	–	[9.6, 11.0]	[11.2, 12.0]	[12.2, 18.6]	[18.8, 20.0]
22π/32	[0.2, 6.2]	6.4	–	[6.6, 8.4]	[8.6, 9.2]	[9.4, 14.6]	[14.8, 20.0]
21π/32	[0.2, 3.4]	3.6	–	[3.8, 4.8]	[5.0, 5.8]	[6.0, 10.2]	[10.4, 20.0]
20π/32	–	[0.2, 1.4]	–	[1.6, 2.0]	[2.2, 2.6]	[2.8, 6.0]	[6.2, 20.0]
19π/32	–	–	–	–	–	–	[0.2, 20.0]
18π/32	–	–	–	–	–	–	[0.2, 20.0]
17π/32	–	–	–	–	–	–	[0.2, 20.0]
16π/32	–	–	–	–	–	–	[0.2, 20.0]

(b) $\alpha = 0.42$.

Table 2
Range of the shear rate k for flow modes in the molecular model for star molecules, $\alpha = 0.42$.

l_2/l	LR	K-Q_2	W-W	DS	FA-y	K-Q_1	FA-z
0.125	[0.2, 4.4]	[4.6, 5.2]	[5.4, 6.8]	–	[7.0, 11.8]	–	[12.0, 20.0]
0.15	[0.2, 4.2]	[4.4, 5.0]	[5.2, 6.2]	–	[6.4, 11.0]	[11.2, 12.8]	[13.0, 20.0]
0.175	[0.2, 3.8]	[4.0, 4.4]	[4.6, 4.8]	–	[5.0, 10.4]	[10.6, 12.4]	[12.6, 20.0]
0.2	[0.2, 3.0]	[10.0, 10.6]	[3.2, 4.4]	–	[4.6, 9.8]	[10.8, 11.2]	[11.4, 20.0]
0.225	[9.8, 11.6]	[0.2, 1.8], [9.2, 9.6]	[2.0, 3.0]	–	[3.2, 9.0]	–	[11.8, 20.0]
0.25	[8.8, 12.6]	[0.2, 1.0]	[1.2, 1.8]	–	[2.0, 8.6]	–	[12.8, 20.0]
0.275	[8.4, 13.4]	–	–	[0.2, 2.4]	[2.6, 8.2]	–	[13.6, 20.0]

significantly larger than the transition value.

In contrast, when the molecular shape parameters are in or very close to the B region, the flow mode sequences are sensitively dependent on the these parameters. Two flow modes, K-Q_1 and DS, are only observed in this case. Moreover, flow modes that appear at low shear rates may now appear at high shear rates. Compared with the flow mode sequences in the N_2 region, where the shear is the only driving force of biaxiality, in the B region, both the molecular interaction and the shear generate biaxiality. Thus, the balance between them can be delicate, leading to diverse flow mode sequences.

4.2.2. Tensor model

We only examine the bent-core molecules using the tensor model. The range of shear rates for each flow mode in tensor models is listed in Table 3a and b. For $\theta = 19\pi/32$ and $\alpha = 0.5$, the flow modes are

DS: [0, 8.4], K-Q_1: [8.6, 16.8], FA-z: [17.0, 20.0].

We compare the results of tensor model with molecular model. Although under different shape parameters, we can observe all the flow modes found in the molecular model. For $16 \le j \le 18$, the only mode FA-z is the same as molecular model. This is also the case for $j = 19$ and $\alpha = 0.42$. For $j = 19$ and $\alpha = 0.5$, the DS takes the place of K-Q_2, while the K-Q_1 and FA-z coincide with the molecular model. For $j = 20$, the sequence in the tensor model covers that in the molecular model, with the extra LR for $\alpha = 0.42$ and W-A for $\alpha = 0.5$. For $21 \le j \le 23$, the tensor model captures only the modes occurring at lower shear rate in the molecular model. Specifically, we do not observe W-W, FA-y and FA-z for the three j, and W-A for $j = 23$ and $\alpha = 0.5$. Some missing modes in molecular model are exhibited, including T for $\alpha = 0.42$ and $j = 22, 23$, K-Q_2 for $\alpha = 0.5$ and $j = 21$, and LR for $\alpha = 0.5$ and $j = 23$.

For the rod-like molecules, the tensor model with Bingham closure has been examined and compared with the molecular model. The results (see [20,45]) suggest that the tensor model works better when α is near the isotropic-nematic transition value, and at low shear rate. This is also observed in our results for bent-core molecules for $20 \le j \le 23$. Because the isotropic–nematic transition value increases as θ decreases, the α we choose is nearer to the isotropic-nematic transition value for $j = 20$ than $21 \le j \le 23$. Indeed, for $j = 20$, the flow mode sequence in tensor model better reflects that in molecular model.

4.3. Discussion

We compare our model and the results with those in [33], where simulation is done for a molecular model.

From the modeling viewpoint, the limitation of [33] is that the coefficients are derived using distinct molecular architecture, meanwhile containing phenomenological coefficients, as stated in that work. Such a model is good enough if we only aim to describe some flow patterns of biaxial molecules. However, it does not suffice if we aim to build connections between molecular architecture and flow pattern, because the molecular architecture is differentiated solely by the coefficients. This aim is attained in the current work by deducing all the coefficients from the same molecular architecture. This feature proves to be crucial, as both experiments and our numerical results evidence that the macroscopic behavior may vary significantly with a small change of molecular architecture.

We now discuss the value of other tensors. We first look at $\boldsymbol{p}$ describing the polar order, which is not considered in [33]. It is incorporated in our model, and the numerical results show that $\boldsymbol{p} = 0$. This is actually a stronger claim than merely ignoring it that the polar order is vanishing in homogeneous flow with hardcore molecular interaction. With other interactions, however, the polar order may

Table 3
Range of the shear rate k for flow modes in the tensor model for bent-core molecules.

θ	LR	K-Q_2	T	W-A	W-W	FA-y	FA-z
23π/32	[0.2, 12.2]	[12.4, 19.2]	[19.4, 20.0]	–	–	–-	–
22π/32	[0.2, 8.6]	[8.8, 13.0]	[13.2, 14.4]	[14.6, 20.0]	–	–	–
21π/32	[0.2, 4.8]	[5.0, 7.4]	[7.6, 8.6]	[8.8, 20.0]	–	–	–
20π/32	[0.2, 1.4]	[1.6, 3.0]	–	[3.2, 5.8]	[6.0, 14.6]	[14.8, 19.6]	[19.8, 20.0]
18π/32	–	–	–	–	–	–	[0.2, 20.0]
17π/32	–	–	–	–	–	–	[0.2, 20.0]
16π/32	–	–	–	–	–	–	[0.2, 20.0]

(a) $\alpha = 0.5$.

θ	LR	K-Q_2	T	W-A	W-W	FA-y	FA-z
23π/32	[0.2, 7.4]	[7.6, 10.4]	[10.6, 12.0]	[12.2, 20.0]	–	–	–
22π/32	[0.2, 4.4]	[4.6, 6.6]	[6.8, 7.4]	[7.6, 20.0]	–	–	–
21π/32	[0.2, 1.8]	[2.0, 3.4]	–	[3.6, 20.0]	–	–	–
20π/32	[0.2, 0.6]	[0.8, 1.0]	–	[1.2, 1.8]	[2.0, 7.4]	[7.6, 10.4]	[10.6, 20.0]
19π/32	–	–	–	–	–	–	[0.2, 20.0]
18π/32	–	–	–	–	–	–	[0.2, 20.0]
17π/32	–	–	–	–	–	–	[0.2, 20.0]
16π/32	–	–	–	–	–	–	[0.2, 20.0]

(b) $\alpha = 0.42$.

appear. Even when considering the hardcore interaction, although not appearing in homogeneous flows, $\boldsymbol{p}$ shall be significant when studying inhomogenous flows. From the free energy, $\boldsymbol{p}$ emerges through the couplings with the modulation of Q_i (see [42]). In the presence of flow, the modulation of Q_i can be generated by the fluid, which might lower the volume fraction for $\boldsymbol{p}$ to exhibit.

Next, we discuss the mixed moments $< \boldsymbol{m}_i\boldsymbol{m}_j >$, $(i \neq j)$. Generally, we shall have $\langle \boldsymbol{m}_1\boldsymbol{m}_2 \rangle = \langle \boldsymbol{m}_1\boldsymbol{m}_3 \rangle = 0$, because the two orientations ($\boldsymbol{m}_1$, $\boldsymbol{m}_2$, $\boldsymbol{m}_3$) and ($\boldsymbol{m}_1$, $-\boldsymbol{m}_2$, $-\boldsymbol{m}_3$) are not distinguishable for bent-core molecules. When the polar order is not exhibited, we shall also have $\langle \boldsymbol{m}_2\boldsymbol{m}_3 \rangle = 0$. We note that the mixed moments are nonzero in [33], which is inconsistent with the molecular symmetry. In our model, numerical results show they are zero in both molecular and tensor model. This can also be proved directly from the model. Actually, in the tensor model, it is guaranteed by (3.19). In the molecular model, if the equality

$$f(P(\alpha, \beta, \gamma), t) = f(P(\alpha, \beta, \gamma + \pi), t) = f(P(\pi - \alpha, \beta + \pi, \pi - \gamma), t) = f(P(\pi - \alpha, \beta, -\gamma), t)$$

holds for $t = 0$, we can prove that it holds for arbitrary $t > 0$ (see Appendix). We then derive from the above symmetric property that $\langle \boldsymbol{m}_i\boldsymbol{m}_j \rangle = 0$ for $i \neq j$.

5. Concluding remarks

In this work, we establish the molecular model and the tensor model for the dynamics of bent-core molecules and star molecules in incompressible fluid. We assume that the molecule is rigid consisting of spheres. Based on this architecture, we build hardcore molecular interaction and sphere–fluid friction into the model. In this way, we obtain the molecular model fully determined by physical parameters, which clearly reflects the molecular architecture. The tensor model is then derived from the molecular model, with the form and coefficients also determined by molecular symmetry and molecular parameters, respectively. Along with the quasi-equilibrium closure approximation, the tensor model inherits the energy dissipation of the molecular model.

We use both molecular model and tensor model to examine the flow modes in the shear flow problem. In particular, we focus on the effect of bending angle of bent-core molecules, and the length of the extra arm of star molecules. The parameters are chosen to cover the transition between three nematic phases N_2, B and N_3, and not to invade the region of modulated nematic phases. We examine the change of flow modes when the parameters go across the $N_2 - B$ and $B - N_3$ phase boundaries. When the equilibrium phase is N_2, we find the flow modes analogous to the rod-like molecules. When the equilibrium phase is B, we find novel flow modes, and the flow mode sequences are delicately dependent on molecular architecture. The tensor model is able to capture all the flow modes shown by the molecular model. Under our choice of parameters, the flow mode sequence is mostly identical to that in the molecular model for smaller bending angles, and recovers the part of sequence in the molecular model at low shear rate for larger bending angles.

Although we only examined the shear flow problem, both the molecular model and the tensor model are ready for the study of inhomogeneous flows. Also, for the shear flow problem, the model can be applied to other molecules with the same symmetry to carry out extensive investigations of the effect of molecular shape. For the sake of computational efficiency, fast algorithms of closure approximation are worth discussion. Currently we compute the quasi-equilibrium approximation by numerical integration, which is time-consuming. It is possible to seek for fast computational methods, as is done for rod-like molecules [16,25,38]. Besides, the formulation of the tensor model allows us to adopt simpler closure approximations that might be suitable for specific types of flows, which is expected to be done in the future.

Acknowledgment

Pingwen Zhang is partially supported by National Natural Science Foundation of China (Grant no. 11421101 and 11421110001).

Appendix A. Some equalities about the closure

Suppose f is given by (3.19), and Z is defined in (3.20). Direct computation gives

$$\frac{F_{entropy}}{k_B T} = \int \mathrm{d}\nu \rho(\boldsymbol{x}, P) \log \rho(\boldsymbol{x}, P) = \boldsymbol{b}\cdot\boldsymbol{p} + B_1 : Q_1 + B_2 : Q_2 - \log Z, \tag{A.1}$$

and

$$\frac{\partial \log Z}{\partial(\boldsymbol{b}, B_1, B_2)} = \frac{1}{Z}\frac{\partial Z}{\partial(\boldsymbol{b}, B_1, B_2)} = (\boldsymbol{p}, Q_1, Q_2). \tag{A.2}$$

Thus we can deduce that (see [42])

$$\frac{1}{k_B T}\frac{\partial F_{entropy}}{\partial(\boldsymbol{p}, Q_1, Q_2)} = (\boldsymbol{b}, B_1, B_2). \tag{A.3}$$

Moreover, The Jacobian $\frac{\partial(\boldsymbol{p}, Q_1, Q_2)}{\partial(\boldsymbol{b}, B_1, B_2)}$ can be expressed by high-order tensors,

$$\begin{aligned}\frac{\partial(\boldsymbol{p}, Q_1, Q_2)}{\partial(\boldsymbol{b}, B_1, B_2)} &= \frac{\partial^2 \log Z}{\partial(\boldsymbol{b}, B_1, B_2)^2}\\ &= \langle(\boldsymbol{m}_1, \boldsymbol{m}_1\boldsymbol{m}_1, \boldsymbol{m}_2\boldsymbol{m}_2)(\boldsymbol{m}_1, \boldsymbol{m}_1\boldsymbol{m}_1, \boldsymbol{m}_2\boldsymbol{m}_2)\rangle - (\boldsymbol{p}, Q_1, Q_2)(\boldsymbol{p}, Q_1, Q_2)\\ &= \mathrm{cov}(\boldsymbol{m}_1, \boldsymbol{m}_1\boldsymbol{m}_1, \boldsymbol{m}_2\boldsymbol{m}_2).\end{aligned} \tag{A.4}$$

Appendix B. The proof of the energy dissipation law of the tensor model

Now we prove the energy dissipation law, for which we need to rewrite the diffusion terms. From (A.3), we can write

$$\mu = k_B T + \mu_{\boldsymbol{p}}\cdot\boldsymbol{m}_1 + \mu_{Q_1}\colon \boldsymbol{m}_1\boldsymbol{m}_1 + \mu_{Q_2}\colon \boldsymbol{m}_2\boldsymbol{m}_2. \tag{B.1}$$

Here we denote $\mu_{\boldsymbol{p}} = \delta F/\delta \boldsymbol{p}$ etc., and F is the free energy. Thus the terms like (3.9) are rewritten as

$$\begin{aligned}&-\int \mathrm{d}\nu \boldsymbol{m}_1\boldsymbol{m}_1 D_2 L_2^2 f = D_2\int \mathrm{d}\nu f L_2(\boldsymbol{m}_1\boldsymbol{m}_1)L_2(\log f)\\ &= D_2\int \mathrm{d}\nu f\,(-\boldsymbol{m}_1\boldsymbol{m}_3 - \boldsymbol{m}_3\boldsymbol{m}_1)(-\boldsymbol{b}\cdot\boldsymbol{m}_3 - B_1\colon(\boldsymbol{m}_1\boldsymbol{m}_3 + \boldsymbol{m}_3\boldsymbol{m}_1))\\ &= D_2[\boldsymbol{b}\cdot\langle\boldsymbol{m}_3(\boldsymbol{m}_3\boldsymbol{m}_1 + \boldsymbol{m}_1\boldsymbol{m}_3)\rangle + B_1\colon\langle(\boldsymbol{m}_1\boldsymbol{m}_3 + \boldsymbol{m}_3\boldsymbol{m}_1)(\boldsymbol{m}_1\boldsymbol{m}_3 + \boldsymbol{m}_3\boldsymbol{m}_1)\rangle].\end{aligned} \tag{B.2}$$

Now we can rewrite

$$\begin{aligned}-\mathscr{M}_{\boldsymbol{p}} &= D_2[\mu_{\boldsymbol{p}}\cdot\langle\boldsymbol{m}_3\boldsymbol{m}_3\rangle + \mu_{Q_1}\colon(\langle\boldsymbol{m}_1\boldsymbol{m}_3\boldsymbol{m}_3\rangle + \langle\boldsymbol{m}_3\boldsymbol{m}_1\boldsymbol{m}_3\rangle)]\\ &\quad + D_3[\mu_{\boldsymbol{p}}\cdot\langle\boldsymbol{m}_2\boldsymbol{m}_2\rangle + (\mu_{Q_1} - \mu_{Q_2})\colon(\langle\boldsymbol{m}_1\boldsymbol{m}_2\boldsymbol{m}_2\rangle + \langle\boldsymbol{m}_2\boldsymbol{m}_1\boldsymbol{m}_2\rangle)].\\ -\mathscr{M}_{Q_1} &= D_2[\mu_{\boldsymbol{p}}\cdot(\langle\boldsymbol{m}_3\boldsymbol{m}_3\boldsymbol{m}_1\rangle + \langle\boldsymbol{m}_3\boldsymbol{m}_1\boldsymbol{m}_3\rangle)\\ &\quad + \mu_{Q_1}\colon\langle(\boldsymbol{m}_1\boldsymbol{m}_3 + \boldsymbol{m}_3\boldsymbol{m}_1)(\boldsymbol{m}_1\boldsymbol{m}_3 + \boldsymbol{m}_3\boldsymbol{m}_1)\rangle]\\ &\quad + D_3[\mu_{\boldsymbol{p}}\cdot(\langle\boldsymbol{m}_2\boldsymbol{m}_2\boldsymbol{m}_1\rangle + \langle\boldsymbol{m}_2\boldsymbol{m}_1\boldsymbol{m}_2\rangle)\\ &\quad + (\mu_{Q_1} - \mu_{Q_2})\colon\langle(\boldsymbol{m}_1\boldsymbol{m}_2 + \boldsymbol{m}_2\boldsymbol{m}_1)(\boldsymbol{m}_1\boldsymbol{m}_2 + \boldsymbol{m}_2\boldsymbol{m}_1)\rangle].\\ -\mathscr{M}_{Q_2} &= D_1\mu_{Q_2}\colon\langle(\boldsymbol{m}_2\boldsymbol{m}_3 + \boldsymbol{m}_3\boldsymbol{m}_2)(\boldsymbol{m}_2\boldsymbol{m}_3 + \boldsymbol{m}_3\boldsymbol{m}_2)\rangle\\ &\quad + D_3[-\mu_{\boldsymbol{p}}\cdot(\langle\boldsymbol{m}_2\boldsymbol{m}_2\boldsymbol{m}_1\rangle + \langle\boldsymbol{m}_2\boldsymbol{m}_1\boldsymbol{m}_2\rangle)\\ &\quad - (\mu_{Q_1} - \mu_{Q_2})\colon\langle(\boldsymbol{m}_1\boldsymbol{m}_2 + \boldsymbol{m}_2\boldsymbol{m}_1)(\boldsymbol{m}_1\boldsymbol{m}_2 + \boldsymbol{m}_2\boldsymbol{m}_1)\rangle].\\ \mathscr{K}_{\boldsymbol{p}} &= \kappa\colon\left[\langle\boldsymbol{m}_1\boldsymbol{m}_3\boldsymbol{m}_3\rangle + \frac{I_{22}}{I_{11}+I_{22}}\langle\boldsymbol{m}_1\boldsymbol{m}_2\boldsymbol{m}_2\rangle - \frac{I_{11}}{I_{11}+I_{22}}\langle\boldsymbol{m}_2\boldsymbol{m}_1\boldsymbol{m}_2\rangle\right].\\ (\mathscr{N}_{\boldsymbol{p}})_\alpha &= \partial_i\Bigg(\partial_j(\mu_{\boldsymbol{p}})_k\sum_{\sigma=1}^{3}\gamma_\sigma\langle m_{1k}m_{1\alpha}m_{\sigma i}m_{\sigma j}\rangle\\ &\quad + \partial_j(\mu_{Q_1})_{kl}\sum_{\sigma=1}^{3}\gamma_\sigma\langle m_{1k}m_{1l}m_{1\alpha}m_{\sigma i}m_{\sigma j}\rangle\\ &\quad + \partial_j(\mu_{Q_2})_{kl}\sum_{\sigma=1}^{3}\gamma_\sigma\langle m_{2k}m_{2l}m_{1\alpha}m_{\sigma i}m_{\sigma j}\rangle\Bigg).\\ (\mathscr{N}_{Q_1})_{\alpha\beta} &= \partial_i\Bigg(\partial_j(\mu_{\boldsymbol{p}})_k\sum_{\sigma=1}^{3}\gamma_\sigma\langle m_{1k}m_{1\alpha}m_{1\beta}m_{\sigma i}m_{\sigma j}\rangle\\ &\quad + \partial_j(\mu_{Q_1})_{kl}\sum_{\sigma=1}^{3}\gamma_\sigma\langle m_{1k}m_{1l}m_{1\alpha}m_{1\beta}m_{\sigma i}m_{\sigma j}\rangle\\ &\quad + \partial_j(\mu_{Q_2})_{kl}\sum_{\sigma=1}^{3}\gamma_\sigma\langle m_{2k}m_{2l}m_{1\alpha}m_{1\beta}m_{\sigma i}m_{\sigma j}\rangle\Bigg).\\ (\mathscr{N}_{Q_2})_{\alpha\beta} &= \partial_i\Bigg(\partial_j(\mu_{\boldsymbol{p}})_k\sum_{\sigma=1}^{3}\gamma_\sigma\langle m_{1k}m_{2\alpha}m_{2\beta}m_{\sigma i}m_{\sigma j}\rangle\\ &\quad + \partial_j(\mu_{Q_1})_{kl}\sum_{\sigma=1}^{3}\gamma_\sigma\langle m_{1k}m_{1l}m_{2\alpha}m_{2\beta}m_{\sigma i}m_{\sigma j}\rangle\\ &\quad + \partial_j(\mu_{Q_2})_{kl}\sum_{\sigma=1}^{3}\gamma_\sigma\langle m_{2k}m_{2l}m_{2\alpha}m_{2\beta}m_{\sigma i}m_{\sigma j}\rangle\Bigg).\end{aligned}$$

Meanwhile, we rewrite the elastic stress as

$$\begin{aligned}\tau_e &= ck_BT\{\mu_{Q_2}\colon\langle(\boldsymbol{m}_2\boldsymbol{m}_3+\boldsymbol{m}_3\boldsymbol{m}_2)\boldsymbol{m}_2\boldsymbol{m}_3\rangle+\mu_{\boldsymbol{p}}\cdot\langle\boldsymbol{m}_3\boldsymbol{m}_1\boldsymbol{m}_3\rangle\\ &\quad+\mu_{Q_1}\colon\langle(\boldsymbol{m}_1\boldsymbol{m}_3+\boldsymbol{m}_3\boldsymbol{m}_1)\boldsymbol{m}_1\boldsymbol{m}_3\rangle\\ &\quad+\frac{1}{I_{11}+I_{22}}\Big[\mu_{\boldsymbol{p}}\cdot\langle\boldsymbol{m}_2(I_{22}\boldsymbol{m}_1\boldsymbol{m}_2-I_{11}\boldsymbol{m}_2\boldsymbol{m}_1)\rangle\\ &\quad+(\mu_{Q_1}-\mu_{Q_2})\colon\langle(\boldsymbol{m}_1\boldsymbol{m}_2+\boldsymbol{m}_2\boldsymbol{m}_1)(I_{22}\boldsymbol{m}_1\boldsymbol{m}_2-I_{11}\boldsymbol{m}_2\boldsymbol{m}_1)\rangle\Big]\}.\end{aligned}\tag{B.3}$$

From the above equations, we deduce (3.21).

Appendix C. Kirkwood theory

We describe how to calculate the spatial diffusion coefficient matrix $\boldsymbol{J}$ using the Kirkwood theory. Assume that the molecule consists of N spheres. Denote by $\boldsymbol{F}_i$ the force exerted on the sphere i due to hydrodynamic interaction. The Kirkwood theory gives

$$\boldsymbol{V}_i=\sum_j H_{ij}\boldsymbol{F}_j,\tag{C.1}$$

where

$$H_{ij}=\frac{1}{8\pi\eta_0|\hat{\boldsymbol{r}}_{ij}|}\left(I+\frac{\hat{\boldsymbol{r}}_{ij}\hat{\boldsymbol{r}}_{ij}}{|\hat{\boldsymbol{r}}_{ij}|^2}\right),\qquad \hat{\boldsymbol{r}}_{ij}=\hat{\boldsymbol{r}}_j-\hat{\boldsymbol{r}}_i,\qquad j\neq i.\tag{C.2}$$

For $j=i$, we adopt the approximation $H_{ii}=I/\tau$ [10], where I is the identity matrix. We choose $\tau=32\pi\eta_0 D$. Suppose that a molecule is undergoing a translation in the quiescent fluid with the velocity $\boldsymbol{V}$. Then $\boldsymbol{V}_i=\boldsymbol{V}$. On the other hand, the total hydrodynamic force shall be identical to the force that stems from the thermodynamic potential. Thus we have

$$\sum_i \boldsymbol{F}_i=-\nabla\mu.\tag{C.3}$$

From (C.1) and (C.3), we can deduce the relation of $\boldsymbol{V}$ and $\nabla\mu$. Define $H\in\mathbb{R}^{3N\times 3N}$, $L\in\mathbb{R}^{3\times 3N}$ and $\boldsymbol{F}\in\mathbb{R}^{3N}$ by

$$H=\begin{pmatrix}H_{11}&\cdots&H_{1N}\\ \vdots&&\vdots\\ H_{N1}&\cdots&H_{NN}\end{pmatrix},\quad L=\begin{pmatrix}\underbrace{I,I,\ldots,I}_{N}\end{pmatrix},\quad \boldsymbol{F}=\begin{pmatrix}\boldsymbol{F}_1\\ \vdots\\ \boldsymbol{F}_N\end{pmatrix}.$$

Then we can rewrite (C.1) and (C.3) as

$$H\boldsymbol{F}=L^T\boldsymbol{V},\quad L\boldsymbol{F}=-\nabla\mu.$$

Therefore, we can solve that

$$\boldsymbol{V}=-(LH^{-1}L^T)^{-1}\nabla\mu.$$

Thus, $\boldsymbol{J}=(LH^{-1}L^T)^{-1}$.

For bent-core molecules, we use a discrete version of (2.37), namely to view the molecule as consisting of $1+N=1+1/\eta$ spheres located at

$$\hat{\boldsymbol{r}}_j=l(\frac{1}{4}-|s_j|)\cos\frac{\theta}{2}\boldsymbol{m}_1+ls_j\sin\frac{\theta}{2}\boldsymbol{m}_2,\tag{C.4}$$

where $s_j=j/N$, $-N/2\le j\le N/2$. Using this molecular architecture we arrive at (2.41).

Appendix D. Symmetry of the molecular model in homogeneous case

We investigate the Smochulowski equation in the shear flow,

$$\frac{\partial f(P,t)}{\partial t}=L\cdot[(D_0\boldsymbol{I}^{-1})(k_BTLf+fLV)]-L\cdot(\boldsymbol{g}f),\tag{D.1}$$

where g is given by (2.34), V is given by (3.4) and (3.1)–(3.3) without gradient terms. We will prove that if the equality

$$\begin{aligned}f(P(\alpha,\beta,\gamma),t)&=f(P(\alpha,\beta,\gamma+\pi),t)=f(P(\pi-\alpha,\beta+\pi,\pi-\gamma),t)\\ &=f(P(\pi-\alpha,\beta,-\gamma),t)\end{aligned}$$

holds for $t=0$, then it holds for $t>0$.

We only prove the first equality, because the other two follow exactly the same way. By (2.7), for arbitrary u, we have

$$\begin{aligned}(L_1u)(P(\alpha,\beta,\gamma),t)&=L_1(u(P(\alpha,\beta,\gamma+\pi),t)),\\ (L_2u)(P(\alpha,\beta,\gamma),t)&=-L_2(u(P(\alpha,\beta,\gamma+\pi),t)),\\ (L_3u)(P(\alpha,\beta,\gamma),t)&=-L_3(u(P(\alpha,\beta,\gamma+\pi),t)).\end{aligned}$$

We then examine the symmetry of right-hand terms at $t=0$. By the symmetry of f, we also have $V(P(\alpha,\beta,\gamma),0)=V(P(\alpha,\beta,\gamma+\pi),0)$. Thus, we can verify that for the diffusion term,

$$[L\cdot((D_0\boldsymbol{I}^{-1})(k_BTLf + fLV))](P(\alpha, \beta, \gamma), 0)$$
$$= [L\cdot((D_0\boldsymbol{I}^{-1})(k_BTLf + fLV))](P(\alpha, \beta, \gamma + \pi), 0).$$

For the convection term, write $\boldsymbol{g} = \sum_{i=1}^{3} (\kappa: \alpha_i)\boldsymbol{m}_i$. It is straightforward to verify that

$$\alpha_1(P(\alpha, \beta, \gamma), 0) = \alpha_1(P(\alpha, \beta, \gamma + \pi), 0),$$
$$\alpha_2(P(\alpha, \beta, \gamma), 0) = -\alpha_2(P(\alpha, \beta, \gamma + \pi), 0),$$
$$\alpha_3(P(\alpha, \beta, \gamma), 0) = -\alpha_3(P(\alpha, \beta, \gamma + \pi), 0).$$

Hence,

$$[L\cdot(\boldsymbol{g}f)](P(\alpha, \beta, \gamma), 0) = [L\cdot(\boldsymbol{g}f)](P(\alpha, \beta, \gamma + \pi), 0).$$

Therefore, $f(P(\alpha, \beta, \gamma), t)$ and $f(P(\alpha, \beta, \gamma + \pi), t)$ are governed by the same equation. Since they are equal at $t = 0$, it is also the case for any $t > 0$.

References

[1] B.R. Acharya, A. Primak, S. Kumar, Biaxial nematic phase in bent-core thermotropic mesogens, Phys. Rev. Lett. 92 (2004) 145506.
[2] S.G. Advani, C.L. Tucker III, The use of tensors to describe and predict fiber orientation in short fiber composites, J. Rheol. 31 (8) (1987) 751–784.
[3] S.G. Advani, C.L. Tucker III, Closure approximations for three-dimensional structure tensors, J. Rheol. 34 (3) (1990) 367–386.
[4] A.N. Beris, B.J. Edwards, Thermodynamics of Flowing Systems with Internal Microstructure, Oxford University Press, 1994.
[5] F. Bisi, E.G. Virga, E.C.G. et al., Universal mean-field phase diagram for biaxial nematics obtained from a minimax principle, Phys. Rev. E 73 (2006) 051709.
[6] V. Borshch, Y.-K. Kim, J. Xiang, M. Gao, A. Jákli, V.P. Panov, J.K. Vij, C.T. Imrie, M.G. Tamba, G.H. Mehl, O.D. Lavrentovich, Nematic twist-bend phase with nanoscale modulation of molecular orientation, Nat. Commun. 4 (2013) 2635.
[7] H. Brand, H. Pleiner, Hydrodynamics of biaxial discotics, Phys. Rev. A 24 (1981) 2777.
[8] C.V. Chaubal, L.G. Leal, A closure approximation for liquid-crystalline polymer models based on parametric density estimation, J. Rheol. 42 (1) (1998) 177–201.
[9] D. Chen, J.H. Porada, J.B. Hooper, A. Klittnick, Y. Shen, M.R. Tuchband, E. Korblova, D. Bedrov, D.M. Walba, M.A. Glaser, J.E. Maclennan, N.A. Clark, Chiral heliconical ground state of nanoscale pitch in a nematic liquid crystal of achiral molecular dimers, Proc. Natl. Acad. Sci. USA 110 (2013) 15931.
[10] M. Doi, S.F. Edwards, The Theory of Polymer Dynamics, Oxford University Press, 1986.
[11] J. Feng, C.V. Chaubal, L.G. Leal, Closure approximations for the Doi theory: which to use in simulating complex flows of liquid-crystalline polymers? J. Rheol. 42 (5) (1998) 1095–1119.
[12] M.G. Forest, Q. Wang, R. Zhou, The flow-phase diagram of Doi–Hess theory for sheared nematic polymers II: finite share rates, Rheol. Acta. 44 (1) (2004) 80–93.
[13] M.G. Forest, Q. Wang, R. Zhou, The weak shear kinetic phase diagram for nematic polymers, Rheol. Acta. 43 (1) (2004) 17–37.
[14] M.G. Forest, R. Zhou, Q. Wang, Kinetic structure simulations of nematic polymers in plane couette cells. II: in-plane structure transitions, Multiscale Model. Simul. 4 (4) (2005) 1280–1304.
[15] C. Greco, A. Ferrarini, Entropy-Driven chiral order in a system of achiral bent particles, Phys. Rev. Lett. 115 (2015) 147805.
[16] M. Grosso, P.L. Maffettone, F. Dupret, A closure approximation for nematic liquid crystals based on the canonical distribution subspace theory, Rheol. Acta 39 (3) (2000) 301–310.
[17] J. Han, Y. Luo, W. Wang, P. Zhang, Z. Zhang, From microscopic theory to macroscopic theory: a systematic study on modeling for liquid crystals, Arch. Rat. Mech. Anal. 215 (2015) 741.
[18] E.J. Hinch, L.G. Leal, Constitutive equations in suspension mechanics. part II. approximation forms for a suspension of rigid particles affected by brownian rotations, J. Fluid Mech. 76 (1976) 187–208.
[19] P. Ilg, I.V. Karlin, M. Kröger, H. C. Öttinger, Canonical distribution functions in polymer dynamics. (II). liquid-crystalline polymers, Physica A 319 (2003) 134–150.
[20] J. S. CintraJr., C.L.T. III, Orthotropic closure approximations for flow-induced fiber orientation, J. Rheol. 39 (6) (1995) 1095.
[21] R.G. Larson, Arrested tumbling in shearing flows of liquid-crystal polymers, Macromolecules 23 (1990) 3983–3992.
[22] R.G. Larson, H. C. Öttinger, Effect of molecular elasitcity on out-of-plane orientations in shearing flows of liquid-crystalline polymers, Macromolecules 24 (1991) 6270–6282.
[23] F.M. Leslie, Theory of flow phenomena in liquid crystals, Adv. Liq. Cryst. 4 (1979) 1–81.
[24] M. Liu, Hydrodynamic theory of biaxial nematics, Phys. Rev. A 24 (1981) 2720.
[25] Y. Luo, J. Xu, P. Zhang, A fast algorithm for the moments of bingham distribution, J. Sci. Comput. (2017). https://doi.org/10.1007/s10915-017-0589-2.
[26] L.A. Madsen, T.J. Dingemans, M. Nakata, E.T. Samulski, Thermotropic biaxial nematic liquid crystals, Phys. Rev. Lett. 92 (2004) 145505.
[27] G. Marrucci, F. Greco, A molecular approach to the polydomain structure of LCPs in weak shear flows, J. Non Newton. Fluid Mech. 44 (1992) 1–13.
[28] C. Meyer, G.R. Luckhurst, I. Dozov, Flexoelectrically driven electroclinic effect in the twist-Bend nematic phase of achiral molecules with bent shapes, Phys. Rev. Lett. 111 (2013) 067801.
[29] T. Qian, P. Sheng, Generalized hydrodynamic equations for nematic liquid crystals, Phys. Rev. E 58 (1998) 7475–7485.
[30] W.M. Saslow, Hydrodynamics of biaxial nematics with arbitrary nonsingular textures, Phys. Rev. A 25 (1982) 3350.
[31] S.M. Shamid, D.W. Allender, J.V. Selinger, Predicting a polar analog of chiral blue phases in liquid crystals, Phys. Rev. Lett. 113 (2014) 237801.
[32] S.M. Shamid, S. Dhakal, J.V. Selinger, Statistical mechanics of bend flexoelectricity and the twist-bend phase in bent-core liquid crystals, Phys. Rev. E 87 (2013) 052503.
[33] S. Sircar, J. Li, Q. Wang, Biaxial phases of bent-core liquid crystal polymers in shear flows, Comm. Math. Sci. 8 (2010) 697–720.
[34] S. Sircar, Q. Wang, Shear-induced mesostructures in biaxial liquid crystals, Phys. Rev. E 78 (2008) 061702.
[35] S. Sircar, Q. Wang, Dynamics and rheology of biaxial liquid crystal polymers in shear flow, J. Rheol. 53 (2009) 819–858.
[36] H. Takezoe, Y. Takanishi, Bent-core liquid crystals: their mysterious and attractive world, Jpn. J. Appl. Phys. 45 (2006) 597–625.
[37] E.G. Virga, Double-well elastic theory for twist-bend nematic phases, Phys. Rev. E 89 (2014) 052502.
[38] H. Wang, K. Li, P. Zhang, Crucial properties of the moment closure model FENE-QE, J. Non Newton. Fluid Mech. 150 (2) (2008) 80–92.
[39] Q. Wang, Comparative studies on closure approximations in flows of liquid crystal polymers: i. elongational flows, J. Non Newton. Fluid Mech. 72 (2–3) (1997) 141–162.
[40] Q. Wang, W. E, C. Liu, P. Zhang, Kinetic theory for flows of nonhomogeneous rodlike liquid crystalline polymers with a nonlocal intermolecular potential, Phys. Rev. E 65 (2002) 051504.
[41] E.P. Wigner, Group Theory and its Application to the Quantum Mechanics of Atomic Spectra, Academic Press, New York, 1959.
[42] J. Xu, F. Ye, P. Zhang, A tensor model for nematic phases of bent-core molecules based on molecular theory, Submitted to Multiscale Model. Simul. (2016), arXiv:1408:3722v2.
[43] J. Xu, P. Zhang, From microscopic theory to macroscopic theory — symmetries and order parameters of rigid molecules, Sci. China Math. 57 (2014) 443–468.
[44] J. Xu, P. Zhang, Calculating elastic constants of bentcore molecules from onsager-theory-based tensor model, Liq. Cryst. (2017), http://dx.doi.org/10.1080/02678292.2017.1290285.
[45] H. Yu, G. Ji, P. Zhang, A nonhomogeneous kinetic model of liquid crystal polymers and its thermodynamic closure approximation, Commun. Comput. Phys. 7 (2) (2010) 383–402.
[46] H. Yu, P. Zhang, A kinetic-hydrodynamic simulation of microstructure of liquid crystal polymers in plane shear flow, J. Non Newton. Fluid Mech. 141 (2007) 116–127.
[47] R. Zhou, M.G. Forest, Q. Wang, Kinetic structure simulations of nematic polymers in plane couette cells. i: the algorithm and benchmarks, Multiscale Model. Simul. 3 (4) (2005) 853–870.